CHALMERS
UNIVERSITY OF TECHNOLOGY

Feasibility study of structural batteries for Electrical Vehicles

Master's thesis in Industrial and Materials Science

Helena Rivera Cueva

Department of Industrial and Material Science
CHALMERS UNIVERSITY OF TECHNOLOGY
Gothenburg, Sweden 2019

MASTER'S THESIS 2019:02

Structural Batteries for Electrical Vehicles

Master's Thesis Report

Helena Rivera Cueva

CHALMERS
UNIVERSITY OF TECHNOLOGY

Department of Industrial and Material Science
Division of Material and Computational Mechanics
Chalmers University of Technology
Gothenburg, Sweden 2019

Feasibility study of structural batteries for electric vehicles

Supervisors: David Carlstedt and Shanghong Duan Department of Industrial and Materials Science
Examiner: Leif Asp, Department of Industrial and Materials Science
Master's Thesis Report
Department of Industrial and Materials Science
Chalmers University of Technology
SE-412 96 Gothenburg
Sweden
Telephone + 46 (0)31-772 1000

Context

List of Figures

List of tables

Abstract

The recent growth in the electric vehicle industry and the fast development of electrical vehicle transportation lead the investigation to new technologies as structural batteries for the electrical vehicle industry. To fulfil the emission agreements, the electric vehicle becomes a promising technology, reducing the emission and CO_2 footprint. However, the relatively low specific energy of this actual lithium-ion technology results in an increase of the vehicle weight. By a combination of a high specific stiffness and energy-storage capabilities within a multifunctional material, the structural power technology, undertakes the duty to bring a solution for this problem. So, this technology endorses weight savings for future vehicle models. In this current study the feasibility analysis was driven to verify the potential of structural power technology. The energy available in the three structural batteries connected in series is analysed. The voltage imbalance between cells was analysed and a technology to minimize this problem was evaluated. The strategy to overcome the cell imbalance was selected and the energy efficiency provided by the battery managements system (BMS). The impact of the selected BMS was assessed in a comparative study between two different BMS technologies. Target energy losses and efficiencies were calculated for both passive and active BMS methods. Significant benefits with an active BMS technology are revelled for structural batteries composites.

Acknowledgments

Firstly, I would like to thank my professor Leif Asp to bring me the opportunity to be a part of this revolutionary research project and have the chance to contribute to the research investigation. Furthermore, I would like to express my sincerest gratitude to David Carlstedt and Shanghong Duan, for their help in during the development of this master thesis. A special thank goes to my parents and friends for their support during the realization of this work, their friendly ears and their encouragement specially at the end of this thesis.

1 Introduction

1.1 Background

Electric vehicles (EVs) have become a viable solution for sustainable road transportation. Due to the improvement of the battery technology, the Battery Electrical Vehicles (BEVs) offer a promising technology for the transition from fossil fuels to emission-free cars. This can provide more efficient means of transportation as well as reduce CO_2 emissions and noise.

The development of the electric vehicle market over the past five years is illustrated in Figure 1. The increased BEV market over the last five years period suggests continuous future growth. Consequently, we expect BEVs to increase their market share and strongly promote the electrification of road transportation.

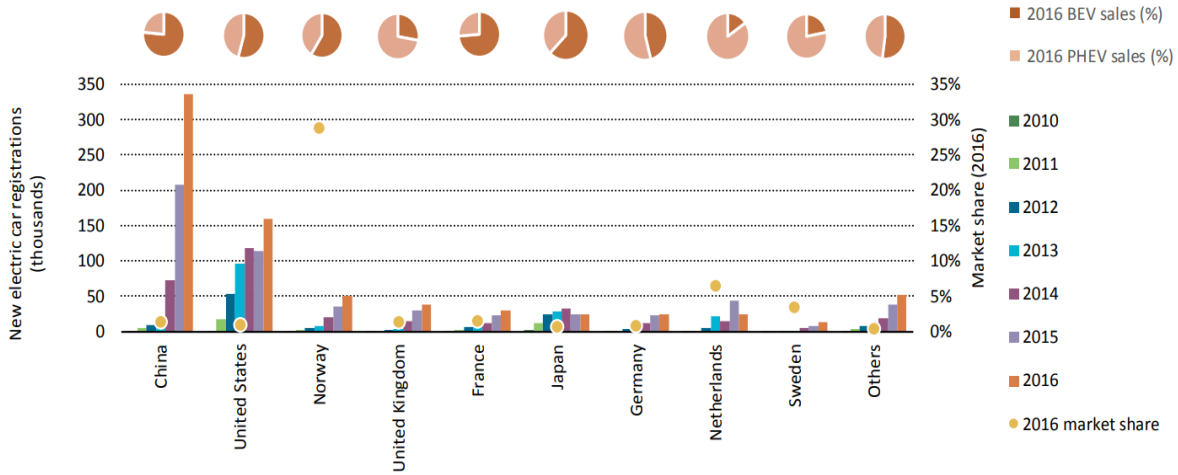

Figure 1: Growth of the electric car sales market [1].

To assist this transition, structural battery composites can find their introduction in BEVs, as they can provide solutions for more energy efficient vehicles. They offer combined mechanical and electrical performance. With such, the monofunctional car structures and electrical devices can be replaced by a multifunctional material in a structure to significantly reduce the mass of the vehicle [1].

The technology of structural batteries is realised by the introduction of both mechanical and electrochemical attributes. In this way, the engineer can devise a multifunctional car structure with the desired stiffness and electrical energy storage properties. Consequently, the introduction of structural batteries offers one route to improve performances of EVs.

This research work focuses on the requirements of the battery management system for the structural battery cells. We aim to develop a robust concept suggesting innovative assembly and control. To validate the new conceptual design diverse tests will be performed to study the electrochemical performance analysing currents, voltage and temperature behaviour during a drive cycle, as well as balance charge and discharge requirements for the battery performance.

To meet the aim of assembling three cells in series, the implementation of the control system will be focused on the minimisation of the imbalance in voltage between cells. We aim to establish a configuration of the system that optimises the structural batteries performance. Lastly, the viability of this system relies on the electrical response of the structural batteries during the battery charge and discharge cycle. Hence, the analysis of these variables during the performance tests will be of interest.

1.2 Structural power technology and multifunctional materials

Ongoing research work is focused on structural batteries and super-capacitors technology, which use polymer composites to build a load-bearing structure, using carbon fibre reinforced as a basis for multifunctional structures. There are four decisive reasons for using polymer composites: their own composition of different layers provides the material a similar structure as a traditional battery; their capability to form into complex shapes; the integration of the electrical connectors into the structure and their ease of being customized [2].

These characteristics make structural battery composites a good option to replace the monofunctional materials. In this context, this research work is addressing the application of multifunctional materials in an EV. In this way, the study work will be driven as one of the first steps of the validation process of this material for use in EVs, in accordance with previous studies that have already provided the performance of this material in aircraft [3].

Previous work done at Imperial London College has provided a feasibility study of structural power composites in aircraft structures and a model to calculate the amount of energy and power required [3]. From these, Scholz determined the mass of material to be replaced by structural supercapacitors composites in an aircraft. This further resulted in alterations in both, wing area

and thickness with the purpose to optimise the design [3]. As a strong point of this research work, applying structural power technology results in an endurance gain and an increase in efficiency. Although the conducted study has demonstrated the potential application of multifunctional materials (MFM) in a successful electric aircraft, in depth studies are required. One particular issue is related to the difficulty to build material demonstrators meeting the requirements on both, specific energy and power densities [3]. The current study follows the research path taken by Scholz [3] adopting MFMs into electric vehicles. Here we evaluate the potential benefits by the introduction of structural battery composites in EVs. We study the effects of different battery design and performance on the range for one type of electric vehicles for a standardised drive cycle.

1.3 Composition of structural batteries

The concept of the structural battery relies on employing individual carbon fibres as a battery electrode. The carbon fibre electrodes are used because of their capability to intercalate lithium ions at very low electrode potential, almost 3.05 V, as well as a way of maximizing superior specific stiffness and strength in structural applications. The microstructure of carbon fibres enables a reversible Li-intercalation reaction between the cathode and anode. This suggests that carbon fibres are a good selection for electrode-reinforcement [4].

The electrochemical performance of structural batteries, which provides the best combination of both electrochemical and structural properties, are made from PAN-based carbon fibres electrodes. Consequently, distinct cases have been evaluated to finally obtain the best combination of carbon fibres properties, for the best performance. A study by Fredi and co-workers [4] showed that intermediate modulus (IM) fibres have the highest capacity values, significantly higher than high-modulus fibres. The recent study showed that the capacity decreases as the crystallite thickness increases [4]. This partly relates to the increase in frustration in the lithium insertion process, inside graphitic parts of the material by the increase of microstructural disorder. In contrast, when this disorder increases even further, the capacity starts to increase. At this point, the lithium insertion is predominantly in the amorphous structure. In a similar way, the fibre strength is controlled by crystal size. Hence, the differences in tensile strength are correlative to the differences in crystal length [4].

Furthermore, the fibre stiffness is controlled by crystal size and orientation, with high oriented large crystals resulting in high stiffness. Previous work from Jacques and co-workers [5]

demonstrated the tensile stiffness of IM fibres to be constant during electrochemical cycling. In addition, the same study showed the capacity of IM fibres (IMS65 and T800) to be unaffected by mechanical tensile loading. Not only is the use of high capacity PAN-carbon fibres crucial for making structural battery composites, but also this high capacity must be retained when the battery is exposed to high mechanical loads [2].

The solid polymer electrolyte (SPE) layer plays an important role in the lithium–ion migration process facilitating it during the charge cycle. Although liquid electrolytes show better conductivity than the solid ones (SPE) the SPE is needed to transfer mechanical loads between the electrode reinforcement [6]. The definition of the material requirements of high mechanical stiffness and lithium ion conductivity is an important issue realising a reliable structural battery. Nevertheless, in this study a liquid electrolyte is used to build the semi-structural batteries aimed for the development of the battery management system.

Given the characteristics of the PAN-carbon fibres, a 3-D structural battery composites concept was proposed by Asp and co-workers [7] and [8]. In this concept, thousands of carbon fibres are coated with a solid polymer electrolyte in a common cathode-doped matrix material constituting the battery, see Figure 2. First tests of this configuration demonstrated the structural battery concept to have a capacity of 10 Wh/kg. Furthermore, the analysis of the concept suggested an energy density of 175 Wh/kg, and a shear modulus of 1 GPa to be within reach. Nevertheless, this research is focussed on the lamina battery concept [6], which was proposed first by Wong et al. [9] and finally demonstrated by Ekstedt [10] and Carlstedt et al. [11]. This structural battery concept will be explained in depth in the next section.

1.4 Configurations of structural batteries

There are two different possible configurations of the structural battery composite as described in the section above. These are the 3D model design and the laminated configuration.

1.4.1 3-D structural battery concept

In the 3-D structural battery composite the fibres act as negative electrodes. These fibres are coated with a thin polymer providing at the same time the functions of a separator for the negative and positive material and electrolyte layer. The polymer matrix is doped with a positive electrode material which acts as the positive electrode in the battery cell. The architecture of the 3D-structural battery is schematically illustrated in Figure 2.

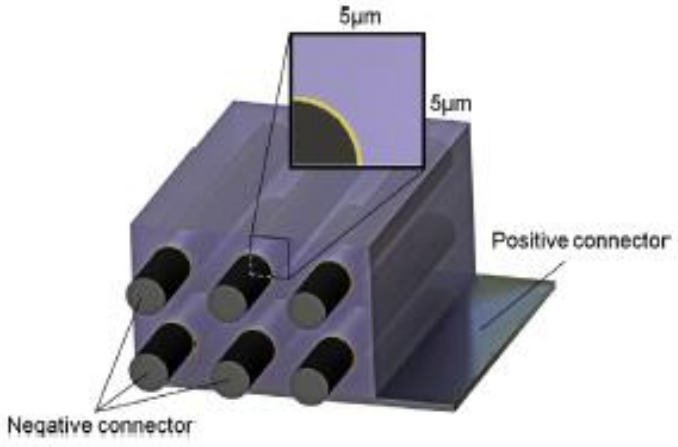

Figure 2: 3-D structural battery design [6].

1.4.2 Laminate structural battery model

For the laminated structural battery, the architecture consists of several layers stacked on top of each other. In this design, each lamina plays a different function inside the battery. The layers act individually as an electrode, collector or separator as shown in Figure 3.

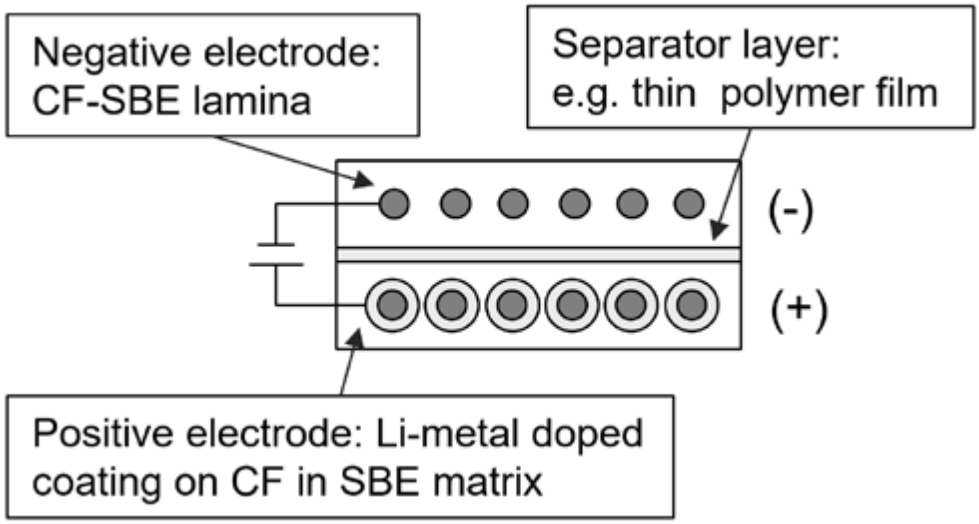

Figure 3: Architecture of a laminated structural battery [11].

This structural battery concept is formed by an electrolyte made from an SPE reinforced with PAN-based carbon fibres as they have shown the highest electrochemical performance [6]. Inside the upper lamina, see Figure 3, carbon fibres represent the negative electrode [11]. The

cathode layer which is illustrated in Figure 3 by the lower lamina, will consist of a coated carbon fibre reinforced SPE. However, the coated material is doped with lithium-metal-oxide based electrode material, which will act as an active positive material inside the layer. As a way to avoid that these different layers do not come in contact and prevent short circuit, an electrical separator layer is placed between the two electrode layers. To mitigate short circuit of the battery cell, the separator layers must be electrically insulating while allowing lithium ion transport between the two layers. Furthermore, the separator layer should be as thin as possible to minimize ohmic losses, and at the same time it must meet the stiffness required to prevent from penetration and allow load transfer.

1.5 Aim and approach

The aim of this study is to determine the effect on drive cycle performance by introducing this kind of structural battery composites in an electric vehicle. The performance of the structural powered EV must be compared with that of EVs monofunctional structures and conventional batteries. This is done with the ambition to demonstrate improvements using this technology on the energy efficiency of future EVs for the automotive industry.

Furthermore, performance targets for the structural battery will be determined for a realistic drive cycle. The performance targets comprise energy density, power density, stiffness, resistivity, and connectivity. The model relies on the energy provided by the structural batteries. Towards this, the profile of the battery discharge process will be defined as a function of the energy supply needed in each time step.

The current study further includes a feasibility study on the structural batteries, to provide input to future structural battery design for EVs. This comes in a comparative study for different cases. This comparative study will give us an overview of the benefits acquired by introducing this new kind of battery in EVs entirely or partially replacing the monofunctional structural system.

In addition, electrochemical test of three battery cells will be performed to provide input to the development of an accurate battery management system. The battery management system will ensure the proper performance of the structural batteries, avoiding a decrease in battery life without compromising the battery electrochemical performance.

The final design for the battery management system (BMS) will rely on a critical assessment of available BMS technologies, considering key factors of the structural battery composites

materials. One of such features is the variability in cell voltage. The proposed BMS design is expected to provide control of the maximum voltage limit for the weakest cell, maximum current drop, charge and discharge time, amount of energy removed from one cell to another, etc. The results obtained from this final part of the study will serve as a guide to optimize future development of structural batteries systems.

1.6 Limitations and scope

The current study addresses the implementation of structural batteries in electric vehicles, replacing some components of the existing electric model, without introducing this new conceptual design with an industrial perspective. In fact, the current work will only comprise the electrical characteristics of the structural battery. In consequence, the mechanical performance will not be addressed. In this comparative study, the values on capacity, battery weight, internal resistance, and maximum discharge rate will be defined by the characteristic values of traditional lithium-ion batteries. These values will establish a reference for comparing with the structural batteries. Furthermore, the requirements of the battery will be established based on the energy storage requirements instead of power requirements from the motor.

The proposed BMS for the structural battery technology will be driven by desired battery performance in a conceptual design. In this perspective, the design process will be driven towards a relevant BMS for the application in mind.

Finally, no physical BMS will be made and nor will the algorithms needed in the design of the BMS be developed in this research work. This research provides a qualitative assessment of the different BMS concepts for structural batteries.

2 Theory

This chapter discusses the theoretical background of the drive cycle analysis. The model is based on a range analysis framework for electrical vehicles [12] and [13]. The introduction of the structural battery composites in a vehicle is assessed for different implementation strategies. For example, in one strategy the structural battery is completely replacing the traditional battery, while in another its only partly replacing the traditional battery. As a reference, the performance of a vehicle powered by a traditional battery system is used. The electrical battery performance

relates to the amount of energy stored and removed from the battery, as well as the estimated requirements from the motor.

2.1 Range analysis

To predict the final distance achieved by the considered electric vehicle, the 'New European Drive Cycle' defined by Pacheco et al. [14] is used. This drive cycle simulates the characteristics and aspects of a standard vehicle travelling in Europe. The range model considers the battery modelling as well as the drag force estimation resulting in more realistic and accurate acquired outcomes. The New European drive cycle (NEDC) is plotted in Figure 4.

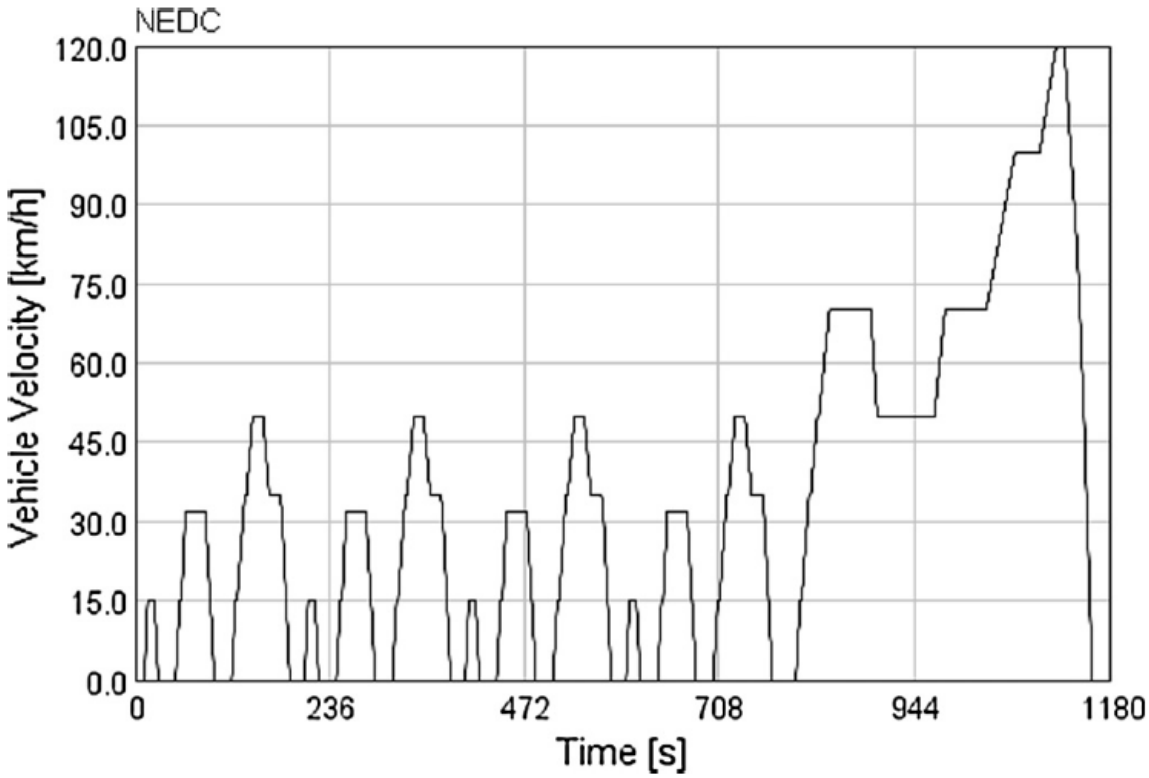

Figure 4: NEDC showing velocity vs time [14].

2.2 Tractive effort

The first step to settle the vehicle performance modelling is to define an equation that allows us to understand the effect of the force propelling the vehicle forward, transmitting this effort to the ground throughout the drive wheels. Overcoming the main opposition forces composed by the rolling resistance, aerodynamic drag and component vehicle's weight acting down the slope or accelerating the vehicle when velocity is not constant, seems essential for this purpose [12].

One can define the total tractive effort as the sum of all these forces as illustrated in Figure 5. Below, the equations that define the forces involved in the tractive effort are described.

Firstly, the rolling resistance results as a response to the friction of the vehicle tyre on the road and is approximately constant, proportional to vehicle mass and does not depend on vehicle speed. Here, the μ_{rr} coefficient is referred to the rolling resistance, and the m is the vehicle mass.

$$F_{rr} = \mu_{rr} mg. \tag{1}$$

Secondly, the aerodynamic drag is a resulting resisting force caused by the movement of the vehicle through the air flow in the surrounding area of the vehicle. In Equation (2), where ρ is the air density, A is the frontal area and v is the velocity of the vehicle and C_d is the drag coefficient.

$$F_{ad} = \frac{1}{2} \rho A C_d v^2. \tag{2}$$

Furthermore, due to the variation on velocity along the drive an additional force is required to be applied, called acceleration force. The acceleration force is calculated as

$$F_{la} = ma, \tag{3}$$

Where m is the vehicle weight and a is the acceleration. The force transmitted to the wheels providing the angular acceleration to the vehicle is defined as

$$F_{wa} = I \frac{G^2}{r^2} a. \tag{4}$$

Here the a is the acceleration, I is the rotor's moment of inertia, G is the gear ratio and r is the tire radius

Consequently, the total tractive force, F_{te} is defined as

$$F_{te} = F_{rr} + F_{ad} + F_{la} + F_{wa}. \tag{5}$$

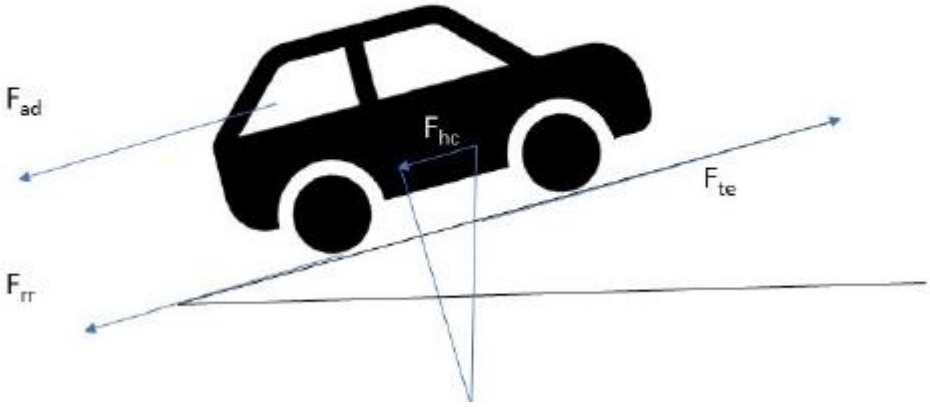

Figure 5: Example of all forces implicated in tractive effort [12].

2.2.1 Power requirements

Having calculated the total tractive force required to move the vehicle the corresponding power required at any instant can be computed. As Equation (6) shows the power required is defined as

$$P_{te} = F_{te} \times v. \tag{6}$$

Knowing the required tractive effort, we can analyse the energy flow in the system predicting the required battery power. The energy flow within the EV system is schematically illustrated in Figure 6.

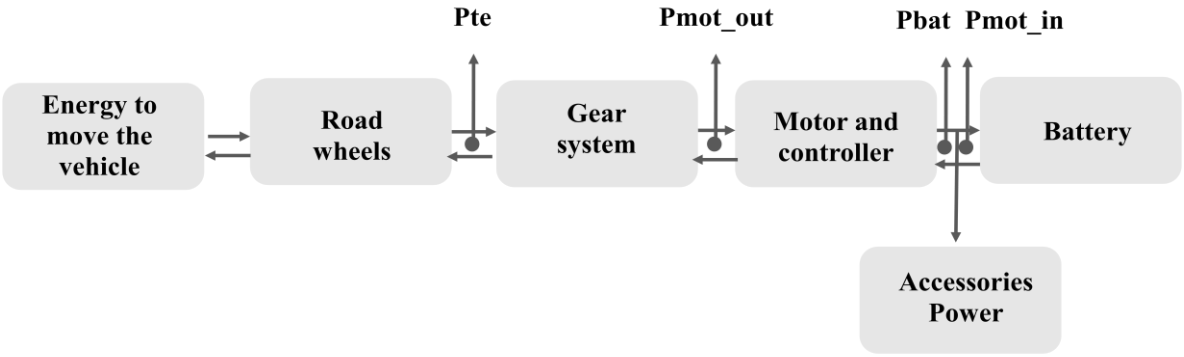

Figure 6: Energy flow within the system [12].

To estimate the total amount of energy delivered by the battery, the energy system flow

needs to be determined. The start point of the energy chain is the power required to move the vehicle defined by Equation (6). To find the way to define the energy supply by the battery at the road, we need to predict all the efficiencies involved in this transformation of energy at all operation points.

The gear efficiency is related to the transmission system connecting the power output of the motor to the vehicle wheels. Assuming this value as a constant is the easiest way to determine the power output from the gear system.

In this context, the losses in motor and controller are usually considered together as a system, so for this case of study is easier to consider the efficiency of both at the system level. Therefore, the inefficiency in gear, control and motor system means the power required from the battery is greater than the power output for the motor. Applying the gear efficiency to the tractive power, we obtain the power for the motor as expressed in Equation (7)

$$P_{mot-out} = \frac{P_{te}}{\eta_g}. \tag{7}$$

Where the η_g is the efficiency of the gear system.

Adding the motor efficiency, we get the power input to the motor.

$$P_{mot-in} = \frac{P_{mot\_out}}{\eta_m}. \tag{8}$$

Here, the η_m represents the motor and controller efficiency considered at the system level.

The power needed to run the auxiliary systems such as lights, indicators, radio, etc. is considered as a constant consumption during the drive. The power required by the motors is provided by the battery pack. Hence the battery power is defined as

$$P_{bat} = P_{mot-in} \tag{9}$$

In this study, we do not consider the energy flow from the regenerate braking system. As a matter of fact, the battery will not be able to receive the incoming energy and normally this function is covered by the super-capacitors in typical electric vehicles.

2.3 Battery requirements

2.3.1 Open circuit voltage

To predict the internal behaviour of the battery cell, we define a number of parameters. To estimate these parameters an equivalent circuit is considered as illustrated in Figure 7.

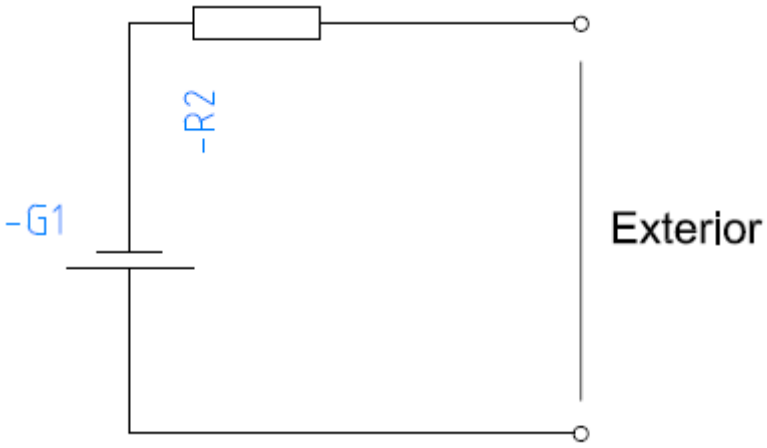

Figure 7: Equivalent internal circuit of a battery model.

First of all, it is necessary to design the equivalent circuit voltage, which is formed by elements with a predictable behaviour [12]. The performance of the internal battery dynamics is defined by resistors, capacitance and inductance elements, assembling the total impedance of the battery. As shown in Figure 7 to simplify the internal battery circuit model, we can approximate the values from the elements involved in the circuit assuming a predicted value for the total battery circuit impedance. With such estimation, we commit a small error that can be accepted for this study case.

Although the equivalent circuit defined seems simple, the values from E and R are not constant values, in other words, their values change over time. In this perspective, we assumed a constant value for battery internal resistance while the open circuit voltage will reach between V_{cell} and $V_{cell} - 0.75$.

The equation for the open circuit voltage of the battery pack is defined as

$$E_0 = N_{serial} \times \left[V_{cell} - [DoD]\right]. \quad (10)$$

Where the N is the total number of cells in series in the entire system, the V_{cell} is the maximum voltage of the cell and DoD is the depth of discharge and gives information about of the state of the battery (amount of energy stored at that time). The assumed values used to model a battery cell are given in Table 1.

Table 1: Assumed characteristic values for the structural battery cell.

Capacity (C_{cell})	3 Ah
Cell voltage (V_{cell})	3.7 V
Mass Cell	0.05 kg
Mass entire pack	600 kg

With this estimation, we can call a function for the open circuit voltage in Equation (10), which will determine the voltage of the battery pack each time. In addition, the condition that the state of charge cannot reach above 0.75 and less than zero is employed. These limits are chosen to avoid compromising the stability of the battery [12].

2.3.2 Capacity definition

It is essential while charging and discharging a battery to be able to predict the effect of the current on the total capacity of the battery. The capacity is obtained by the product of current discharged per time of the discharge cycle time. The capacity is referring to the amount of energy that can be stored in the material.

The specific capacity is defined as

$$C = \int_0^t I \frac{dt}{m}, \tag{11}$$

Where, I is the current, m is the mass of the electrochemical active materials and t represents the time.

The capacities of the negative and positive electrodes in the laminated structural battery are defined as:

$$C_{neg} = C_f \times A_c \times \sum t_{neg} \times V_{f,neg} \times \rho_n, \tag{12}$$

$$C_{pos} = C_P \times A_C \times \sum t_{pos} \times V_{p,pos} \times \rho_p. \tag{13}$$

In Equation (12) and (13), the C_p and C_f are the specific capacity of $LiFePo_4$ and carbon fibre respectively. The A_c defines the total battery cell area in the component, the thickness of both electrolytes are defined as $\sum t_{neg}$ and $\sum t_{pos}$. The volume fraction of fibres in the negative

lamina appears as $V_{f,neg}$ and the volume fraction of the particles in the positive electrode is $V_{p,pos}$**.** Finally, the density of the particles and fibres are defined as ρ_p and ρ_n respectively.

By expression below, the specific capacity of the cell can be defined as:

$$C_{Cell} = \frac{min(C_{neg}, C_{pos})}{W_{Cell}}. \tag{14}$$

Where W_{Cell} is the total weight of the cell, which can be derived issuing a model lamina, with specific thickness, volume fractions and material densities described by Carlstedt et al. [11]. In case of balanced active materials, the differences in capacity are zero, resulting in a maximum specific capacity component.

Once the capacity is estimated, we can define the total cell capacity using the Peukert method. The Peukert method is used for higher current ranges to account for the effects of charge rates on capacity. In this context, the starting point of this model is to define the Peukert capacity, given the following equation

$$C_P = I^k \times T. \tag{15}$$

Where the *k* is assumed to be 1.1 for this study case. This assumption means that when discharging a cell, the capacity does not vary significantly with an increasing C rate. In fact, conventional batteries are within a range of 1 and 1.2 for this value.

For every time step calculations, we define a function for the apparent or effective charge removed from the battery as

$$\delta t \times I^k, \tag{16}$$

Here, the δt is the time step calculation and I is the current flowing in Amperes.

Therefore, we can define the total amount of energy removed from the battery during the *n* step calculating CR_n with the equation

$$CR_{n+1} = CR_n + \frac{\delta t \times I^k}{3600}\ (Ah). \tag{17}$$

The Depth of discharge is a ratio for the energy removed over the original capacity, which at the *n* step of the discharge is defined as

$$DoD = \frac{CR_n}{C_p}. \tag{18}$$

Where the C_p is the Peukert capacity calculated from Equation (15).

2.3.3 Current drop definition

When an electrical vehicle runs at a certain speed, the battery system needs to supply certain energy to the motor. In this case, it is necessary to be able to simulate the operation range of the battery.

The power delivered by the battery is defined as

$$P = E \times I. \tag{19}$$

Where E is the potential and I is the current.

If we replace the value of the nominal voltage of the battery in Equation (19), the power can be expressed in terms of current drop as

$$P = E \times I = (E - IR) \times I = EI - RI^2, \tag{20}$$

Equation (20) is quadratic and is solved with the formula for quadratic equations. Only the negative solution of Equation (19) is considered in accordance with [12].

$$I = \frac{E - \sqrt{E^2 - 4RP}}{2R}, \tag{21}$$

In this case, the limitation of the current is established by the values of the internal resistance, power, and voltage. This limitation is found from the expression

$$E^2 - 4RP > 0 \tag{22}$$

If the expression (22) is not fulfilled, the battery will not be able to deliver the required energy. In other words, this expression defines the limit at which the battery can deliver the motor power.

Continue with the battery modelling, the next step will be to limit the discharge rate ensuring battery integrity. In this case, the maximum value that the battery can reach was estimated by the normal lithium-ion battery data and it was set to at 5 A per cell.

With this final limitation of the current drop, we ensure the proper simulation of the battery performance within the drive cycle.

3 Methodology

As mentioned previously, this study concerns the introduction and management of structural batteries in electric vehicles. Firstly, a comparative study is performed to assess the feasibility of structural batteries as replacement to conventional batteries in EVs. The software

MATLAB will be used to run this study. The results win provide information of the feasibility of structural batteries and the different battery pack structures.

Typically, the performance of the battery packs is controlled by the BMS ensuring the optimization of each cell within the pack and its electrochemical cycling. Indeed, the BMS is crucial for the battery pack structure, and from the perspective of structural batteries becomes essential to improve the system efficiency. Therefore, the definition of the BMS to accomplish the targets for the contrasting study becomes a major purpose within this project.

3.1 Procedure

Firstly, the model is configured for conventional batteries assuming the values for the battery weight and motor voltage from the values for the Tesla model S. Generally, based on a simple cell voltage estimation, the number of cells in series fulfilling the motor's requirements can be established. Once the number of cells in series is defined, the number of cells in parallel can be established by dividing the mass of the entire pack by the mass of each cell and the number of cells in series.

With the values obtained, the battery performance can be defined. In addition, the model can be run to obtain the drive cycle range for each case, the peak current and the total energy removed from the battery pack at the end of the cycle.

We first run a simulation for the conventional battery case. Once the first simulation is run, the same procedure will be adopted to predict the different cases. For the two simulations left, the same parameters are used substituting the related values for the structural batteries in the cases needed. However, in the cases where the structural batteries are implemented, we assume that the battery mass is not included in the vehicle mass. Under the assumption of the structural batteries will replace different parts of the vehicle and provide both the structural and electrical functions. Finally, this simulation process will be repeated for the different cases of study, presented in the Table 2. The table summarises the assumptions made in each case and introduces the input values for the drive cycle.

Table 2: Initial data for the drive range model.

Cases	Conventional Batteries	25% of structural batteries	100% Structural batteries
Total battery mass (kg)	600	600	600
Mass Battery cell (kg)	0.05	0.05	0.05
Cell capacity (Ah)	3	3	3
Total capacity (Ah)	360	360	360
Motor voltage (V)	370	370	370
Cell voltage (V)	3.7	3.7	3.7
Nº cells in series of structural batteries	0	100	100
Nº cells in series of conventional batteries	100	100	0
Nº cells in parallel structural batteries	0	18	120
Nº cells in parallel conventional batteries	120	102	0
Nº cells in total	12000	12000	12000
Cell internal resistance (Ω)	0.02	0.2/0.02	0.2

The three cases listed in Table 2 are described below.

Case 1: Conventional batteries

- Definition of the system weight includes the mass of the conventional batteries.
- Power to feed the motors totally supplied by conventional lithium-ion batteries.
- Internal battery resistance estimated as an average of 0.02 ohm per cell.

Case 2: 25% structural

- Calculation of the system weight for the 25% of the conventional battery mass replaced by the structural battery.
- Power to feed the motors supplied to 25% by structural batteries and 75% by conventional batteries. Ensuring the voltage required by the motor in both cases with the same number of cells in series, resulting in two separated systems in parallel.
- The total internal resistance is estimated by the two internal resistances of the both battery models in parallel.

Case 3: 100 % structural batteries

- Calculation of the system weight for zero conventional battery mass.
- Power to feed motors entirely supplied by structural batteries.
- Internal battery resistance estimated as an average of 0.2 ohm per cell.

In each case, the total internal resistance is calculated as

$$R_{total} = \frac{n_{cells\_serial} R_{Internal\_resistance}}{n_{cells\_parallel}} \tag{23}$$

3.2 Algorithm

The predictive model runs a nested loop in which the relative range of the drive cycle is calculated for each time step of the NEDC cycle. As a starting point for the loop, the simulation reads the velocity data from the NEDC and the parameters presented at the beginning of this chapter. With all this information, the loop runs until the end of the discharge is reached (DoD <0.75), at that time the battery has reached its discharge limit and the loop is stopped to end the drive cycle. In addition, the loop is running to determine the power demand using the calculation

of the tractive force and hence the battery demand. The schedule of the program algorithm is illustrated in Figure 8.

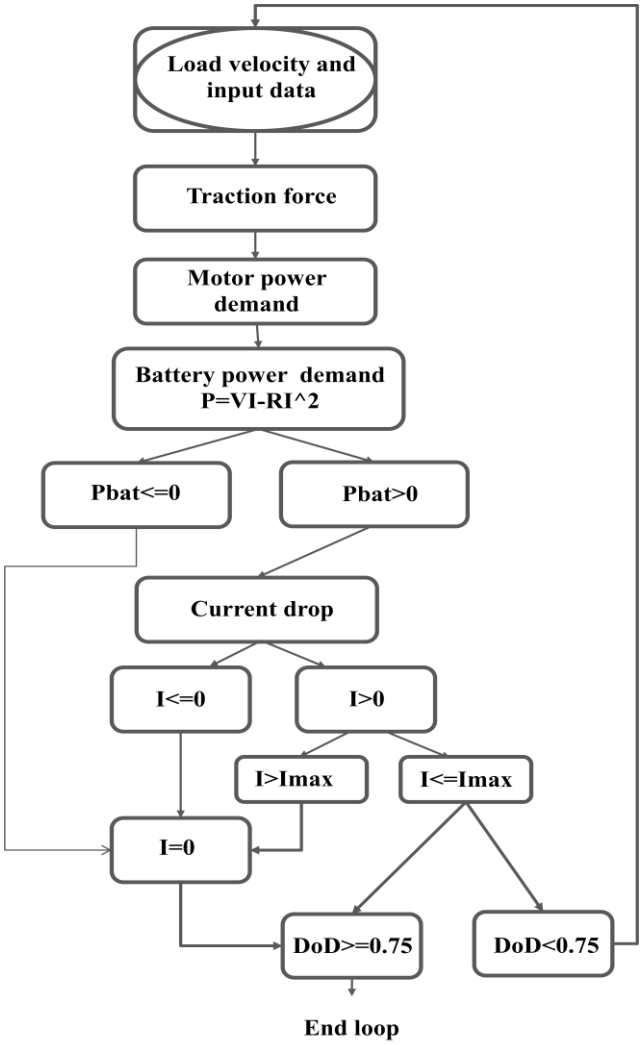

Figure 8: Algorithm schedule.

3.3 Range analysis cases of study

As shown in Table 2, three different cases are studied in this analysis. All cases address the same vehicle basis, assuming the normal values for a car design presented in Table 3, below. These values were computed using the motor and vehicle requirements from the Tesla model S.

Table 3: Motor and vehicle requirements.

Motor Voltage (V)	370
Vehicle weight without battery (kg)	1500
Battery pack mass (kg)	600

3.4 Battery management system for structural batteries technology

The structural battery technology provides important advantages to EVs compared with the conventional lithium-ion batteries. However, there are some disadvantages to overcome in the manufacturing process and performance to strengthen the efficiency of this technology. The main problems of this technology are the imbalance in voltage and capacity between cells, resulting from the high variability in the manufacturing process. To overcome this problem, the BMS offers a solution to improve the performance of this technology within the EV [15].

The main quandaries that come up at the beginning are the imbalance caused by the capacity difference and voltage difference between cells during battery operation. The capacity imbalance between cells consists of a large deviation between cells employed at the end of the discharge. While the voltage imbalance during performance appears when one of the cells connected in series has less capacity than the others. The strongest cells will expose the weakest cell to an overvoltage making the degradation of this cell even further. For this reason, a BMS is suggested to improve the performance of the battery cells and addressing the points below [16].

To ensure the good operation of the structural batteries we will search for a BMS technology able to overcome the following statements

- Battery control: the control system must monitor the battery outputs each time step using sensors, electrical devices, and algorithms.
- Prevent from cell overvoltage: During the charge and discharge process, the system will limit the voltage in cell strings and hence the current flow.
- Estimation of battery SOC: The system needs to be able to predict the battery state of charge.

3.5 BMS strategies

The problem of cell imbalance is mainly caused by internal sources. These internal sources include manufacturing variance in the charge storage volume, internal resistance, and differences in self-discharge rates [16].

The balancing topologies of the BMS are categorized into two main groups; passive and active architectures. Where the passive balancing topology removes the excess charge from the fully charged cells by resistors set in parallel with each cell, until the charge matches those of the lower charged cells within the pack. The active balancing topology uses external circuits to equalize the cells [17].

This chapter discusses some of the different methods proposed in the literature. The several topologies are compared based on their complexity, topology, application and balancing efficiency. The two groups diversify in different topologies based on the elements employed to build the internal architecture. The different strategies for the BMS design are shown in Figure 9.

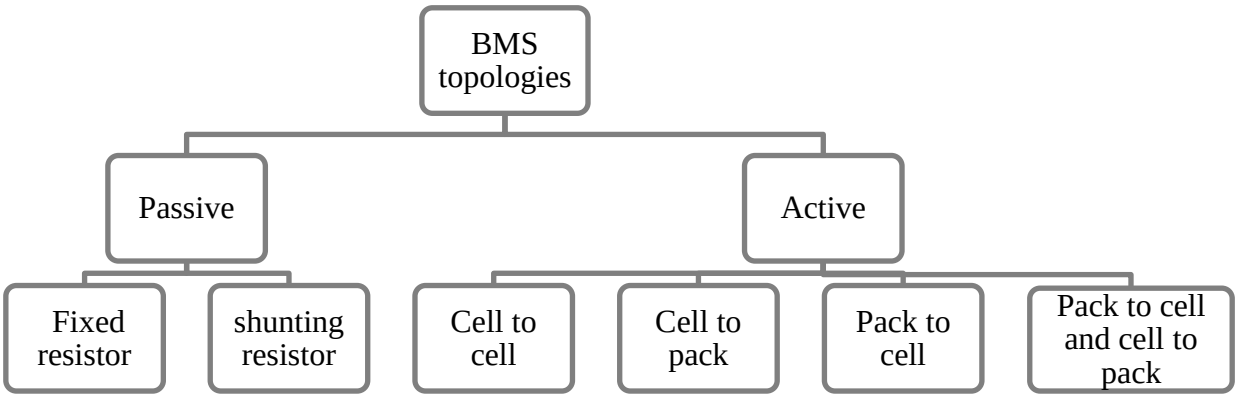

Figure 9: Diagram of BMS topologies.

3.5.1 Passive methods

In the passive balancing methods, no control of the equalization process between cells is used. In fact, these methods can only be used for the lead-acid and nickel-based battery technologies as lithium-ion batteries must not be over-charged [17]. Concerning the energy flow, this technology removes the energy among cells using the bypass method.

This category is subdivided into two main balancing methods, the fixed resistor and the shunting resistor. These methods are briefly described in the Appendix A.

3.5.2 Active methods

Active balancing systems use external circuits to actively move energy between cells with the purpose of equalize them. Hence, they are unique methods that can be implemented in lithium-based batteries [17].

Concerning the energy distribution within the system the active balancing methods can be classified in four categories, formed by cell-to-cell, cell to pack, pack to cell and cells to pack to cell [17]. These can briefly be described as;

- Cell to cell: The energy is conducted from the overcharged cells to the least charged adjacent cells.
- Cell to pack: The energy is moved from the overcharged cell to the whole battery pack.
- Pack to cell: The current is moved from the entire pack to the lower charged cell using galvanic insulated DC/DC converters.
- Cell-to pack-to cell: The current flow is bypassed from the set cell to the whole pack and finally to the target cell or from the set cells to the target cells.

The passive and active methods are described in depth in Appendix A. These methods are considered in the current work to explain the selected BMS topology justified in section below.

Having explained the diverse BMS topologies, we will now establish the technology that suits best the structural batteries technology assembly. To start the selection process, we must first determine selection criteria. The main criteria for assessment of the different topologies are efficiency, application, speed, best effective period and cost. The different topologies are evaluated and assessed in Table A1 to Table A5 presented in Appendix A.

In these tables the benefits and weaknesses of the different BMS technologies are listed. Based on this analysis we select the topology for our study case. Considering, the amount of energy saved, the lower losses of the system and the equalization balancing method of the active topology, the selection fell upon the voltage multiplier seen in Figure 10 which is a pack-to-cell BMS topology. This technology will increase the feasibility and reliability of the structural batteries structure, improving their integration in the EVs. Since, this technology increases the battery cycle while at the same time, prevents from hazards performance avoiding overcharge

and cell imbalance. All these benefits make the integration of the structural batteries in EVs resulting in a highlight interest.

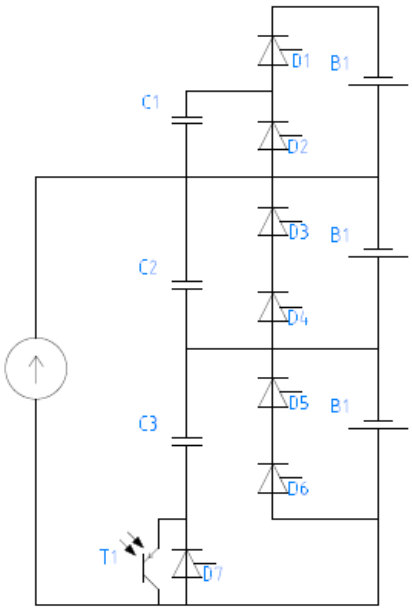

Figure 10: Voltage multiplier architecture.

4 Results

In this chapter, the drive cycle and BMS analysis results are presented and discussed. The BMS results consist of an energetic estimation of the capacity and voltage imbalance between cells, considering the energy transfer path by the selected BMS.

4.1 Drive range analysis results

Here results on the effect of introducing structural batteries in EVs drive cycle explained in section 3.1 for the NEDC are reported. Thereafter, the two cases, 25% of structural batteries and 100% structural batteries completely feeding the motors are analysed.

Table 4: Results from the relative drive range analysis.

Cases	Conventional batteries	25% of structural batteries and lithium-ion	100 % Structural batteries
Energy stored (Ah)	360	360	360
Total mass (kg)	2110	2010	1500
Resistance (Ω)	0.0667	0.0693	0.2167
Relative drive range	1	1.05	1.23
Energy consumed (Ah)	391	387	390
I max demand battery pack (A)	147	140	132
I max demand cell (A)	1.2	0.6	1.1
C_rate (cell)	0.4	0.2	0.4

The results from the drive range analysis are presented in Table 4. The table summarises the results obtained for the different cases showing the differences between them. As shown, introduction of structural batteries has a significant effect on the relative drive range. This ratio shows the difference in distance travelled between the studied cases normalised by the value achieved in the conventional battery case. If we use the structural batteries as the main motor power source, the relative drive range is increased due to the reduced weight caused by structural battery composites to the system. As seen in Table 4, the mass of the vehicle system for case 3, is only 1500 kg, compared to the 2110 kg for the case with conventional batteries. In the case of the 25% of structural batteries feeding the motors the relative drive range is moderately increased when the total mass of the system is moderately reduced to 2010 kg. The next value in which we can see an important divergence, is the internal resistance of the battery pack. The higher value is achieved by the case of the structural batteries feeding the motors due to the high

set up value assumed. Finally, the last difference, appears in the delivered peak current as the distinct cases owns a dissimilar internal resistance. As a result of the difference in the maximum current, the C rate differs between the three cases on the cell level.

Figure 11 illustrates the differences in drive range and system mass for the three cases. As discussed above the longest relative range is found for the 100% structural batteries case correlating to the lowest system weight.

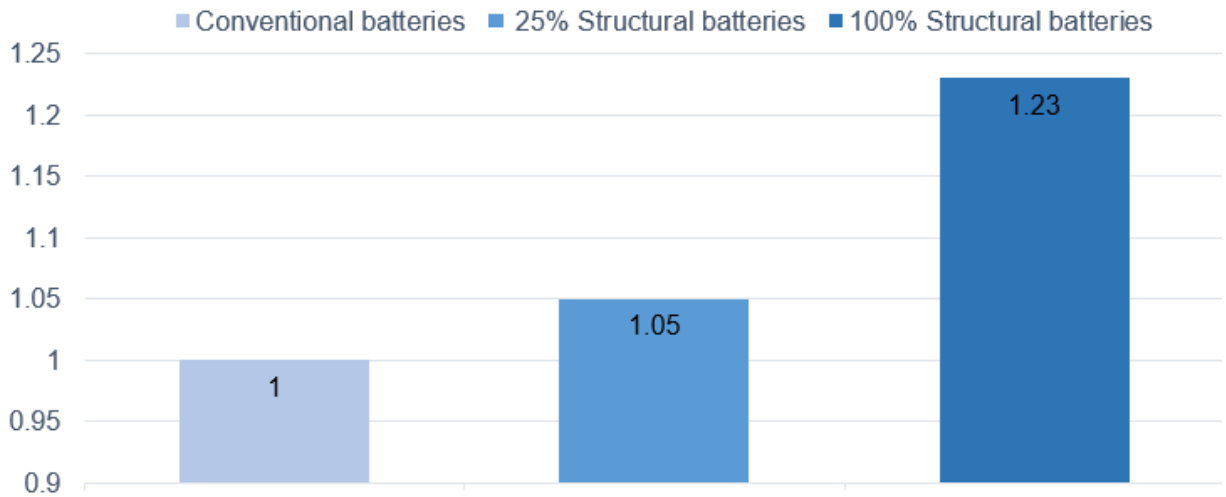

System weight	Conventional batteries	25% structural batteries	100% structural batteries
	2110	2010	1500

Figure 11: Analysis of the relative drive range for the different cases.

Regarding the energy flow characterization, Figure 12 shows the variation in current requirements during the last drive cycle. The graph shows, the fluctuation in delivered current related to the power demand for the case with 100% structural batteries.

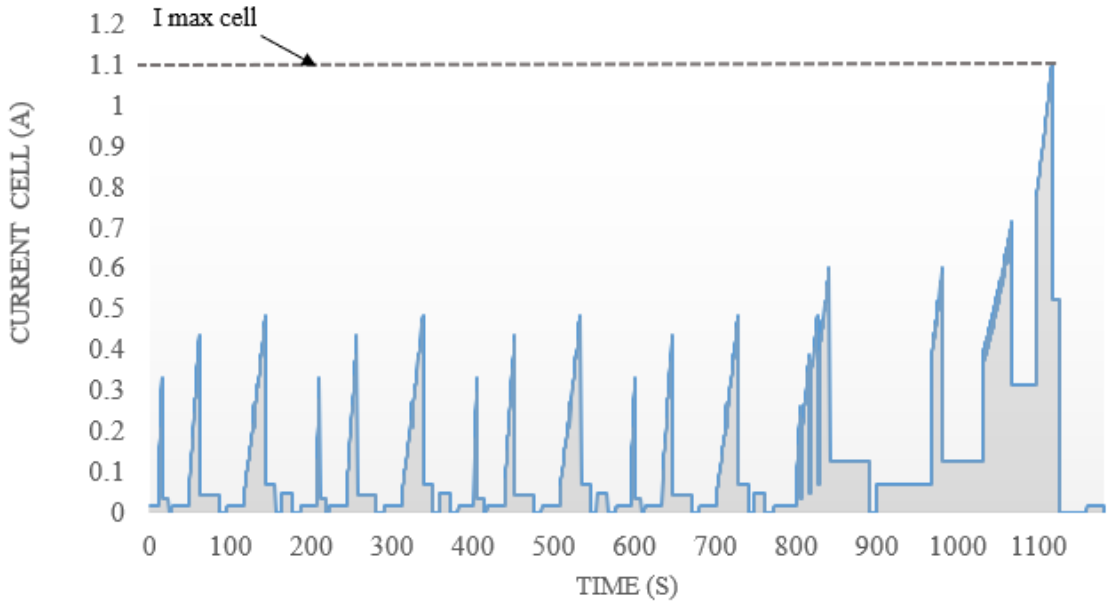

Figure 12: Current fluctuation within the last drive cycle.

As shown in Figure 12, the peak of current is 1.1 Amperes and is reached at 1100 seconds into the drive cycle. Moreover, this graph exhibits the limitation of negative current drop. In case a negative power demand is required, the value of delivered current is established at zero, in accordance with the statements of section 2.3.3.

Furthermore, a parametric study of the influence of the internal resistance on the relative drive range and current peak was performed. The results for an internal resistance ranging from 0.02 to 0.2 ohm are showed in Table 5.

Table 5: Results from the parametric internal resistance study.

R (ohm)	0.02	0.07	0.14	0.2
Relative range	1.25	1.25	1.23	1.23
Imax cell (A)	1.01	1.03	1.06	1.10

Here, we can appreciate a small variation in the value achieved by the relative drive range with internal resistance. Since, the internal resistance varies between cells the delivered current also varies.

4.2 Comparative study of active and passive balancing systems

Here results of a comparative study of different BMS strategies are presented. The analysis is performed on three structural batteries built and tested at Chalmers University of Technology. Three pouch half-cells samples were tested them in the laboratory with a power source providing the power required first to charge the half-cells. The three cells were characterized under galvanostatic conditions and the capacity was measured. In the Table 6, the capacity values of the three different samples is stated.

Table 6: Capacity measured in the three samples

	Sample no. 1	Sample no. 2	Sample no. 3
Capacity half-cells (Ah)	0.0023	0.0018	0.0022

The charge and discharge curves for the three samples are plotted in Figure 13 and Figure 14 respectively. The displayed charge and discharge curves are from the third cycle.

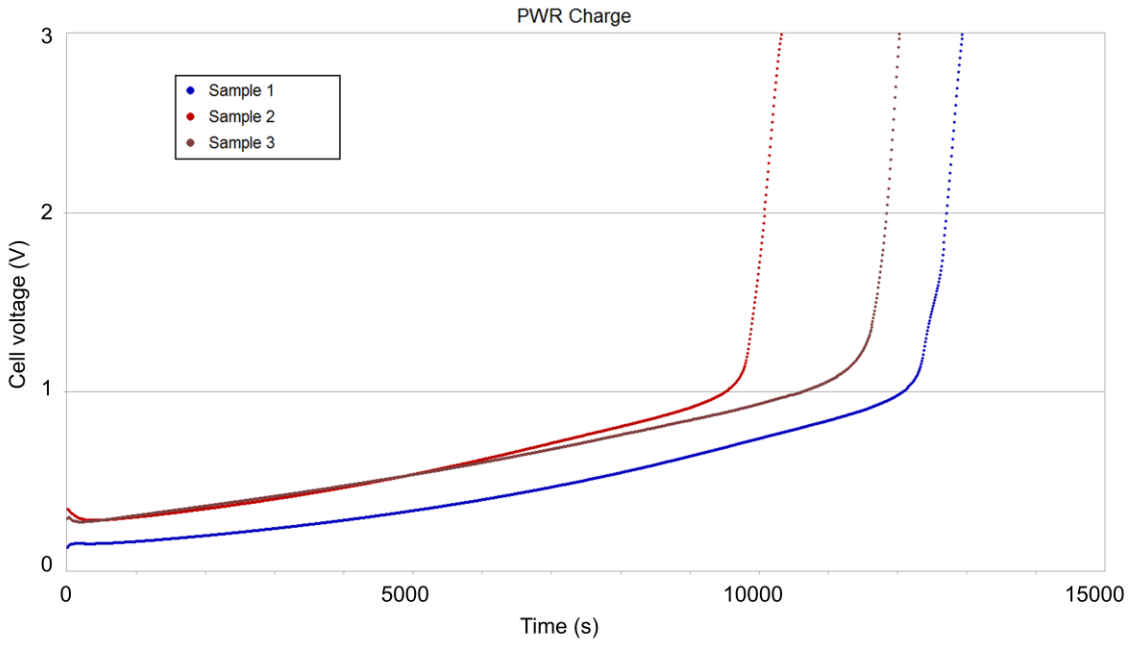

Figure 13: Charge curve for the three samples.

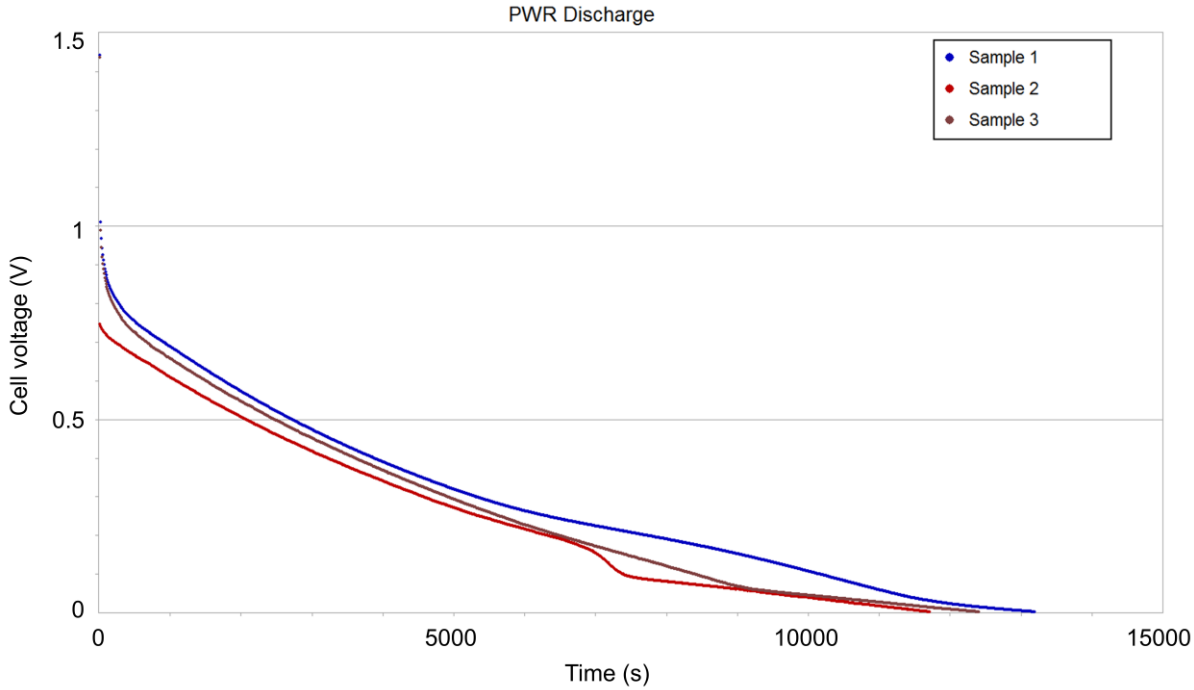

Figure 14: Discharge curve for the three samples.

These plots present the information of capacity stored in the three different samples. In Figure 14 the area under each curve represents the total amount of capacity available in the half-cell. As shown on the Figure 14 the energy available in the sample varies among cells, we can determine the weakest cell among the three samples. In accordance with the data collected from the lab, the half-cell with the lowest energy available is sample no. 2. As seen in Figure 13, sample no. 2 becomes fully charged much quicker than the others. Furthermore, sample no. 2 is the first to finish the discharge process as seen in Figure 14.

Having said all of this, with the data collected from the laboratory we can analyse, the benefits of introducing a voltage multiplier as an active balancing system and compare that with the passive methods.

4.2.1 Results from the passive and active BMS

Given the data collected in the lab, the differences between the two systems are analysed in this section. Figure 15 to Figure 19, present the results for the three battery cells connected in series without use of any battery management system.

Figure 15 shows the state of charge of the three cells at the end of the charge process for the three samples connected in series.

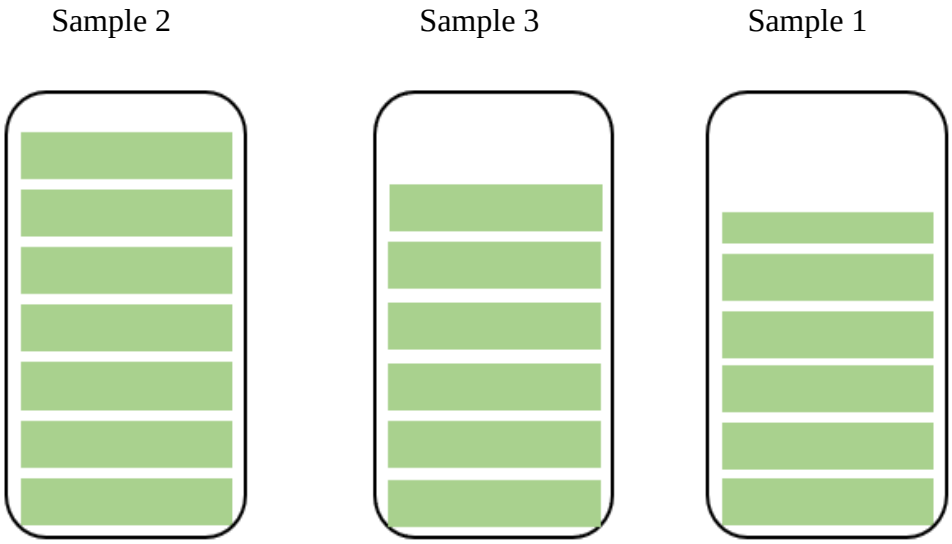

Figure 15: State of charge of the three cells at the end of the charging process.

The charging process is limited by the weakest cell, i.e. no. 2.

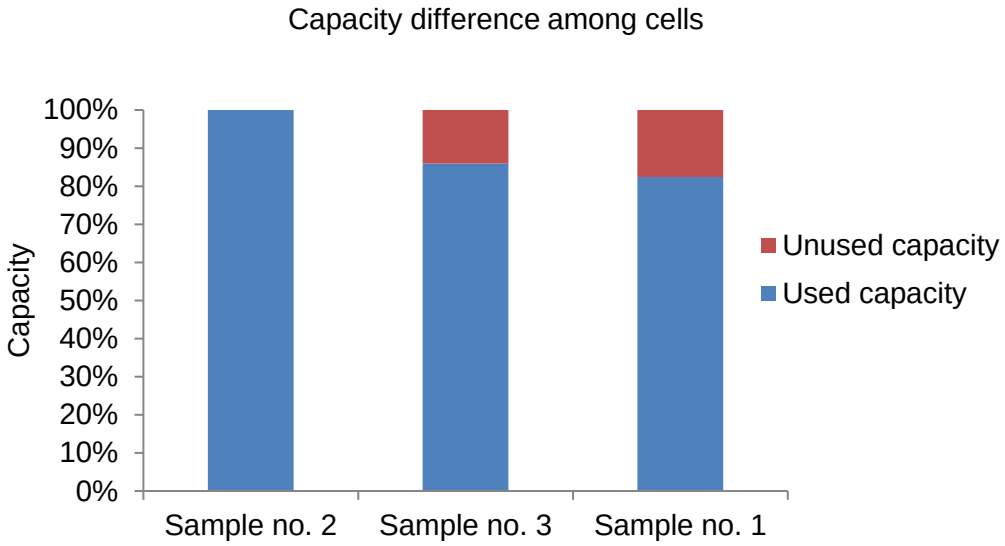

Figure 16: Capacity imbalance between the three samples.

The capacity imbalance among cells is illustrated in Figure 16 were the percentage of unused capacity represents the capacity left in sample no. 1 and no. 2, when the sample no. 2 is completely discharged.

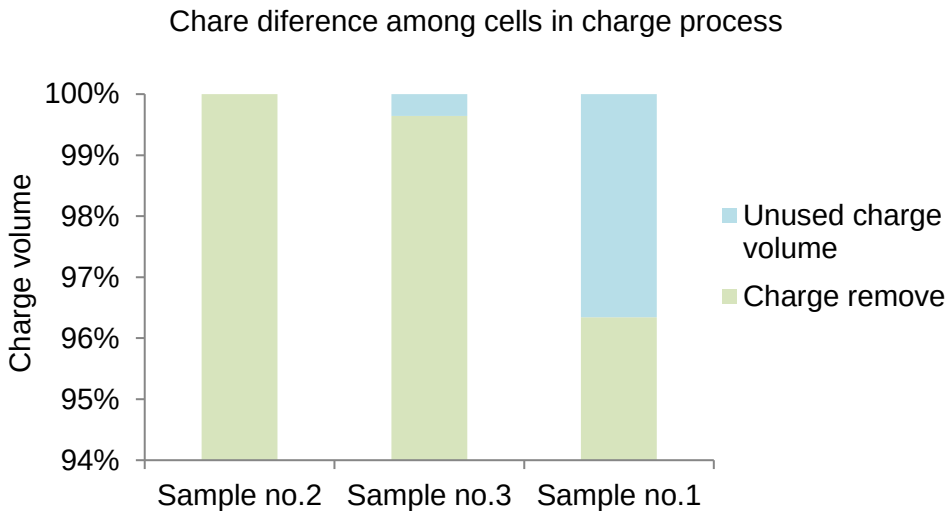

Figure 17: Charge imbalance during charge process.

Figure 17, shows the unused charge volume in the samples no. 1 and no. 3 when sample no. 2 reaches full charge and the charge process is ended.

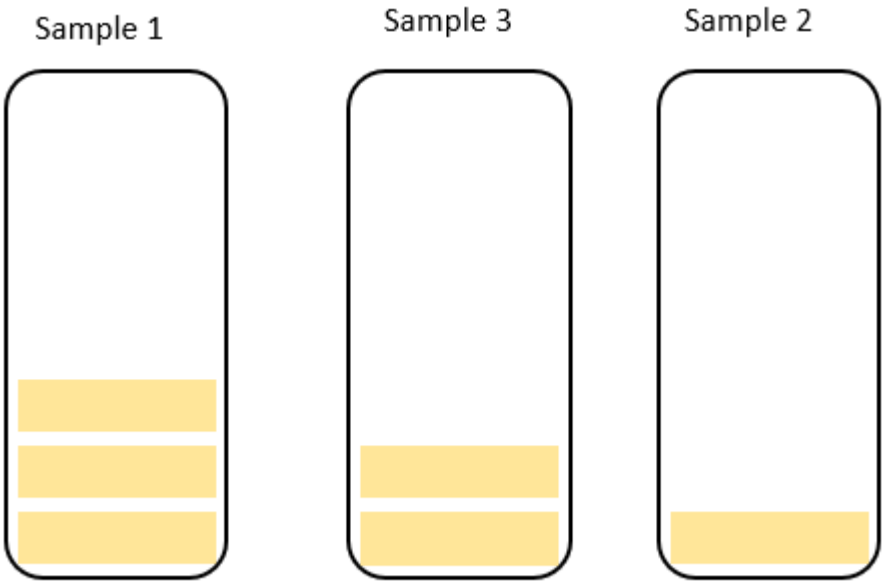

Figure 18: Depth of discharge for the unmanaged system.

Figure 18 illustrates the depth of discharge of sample no. 1 and no. 2 when sample two has reached its minimum voltage level.

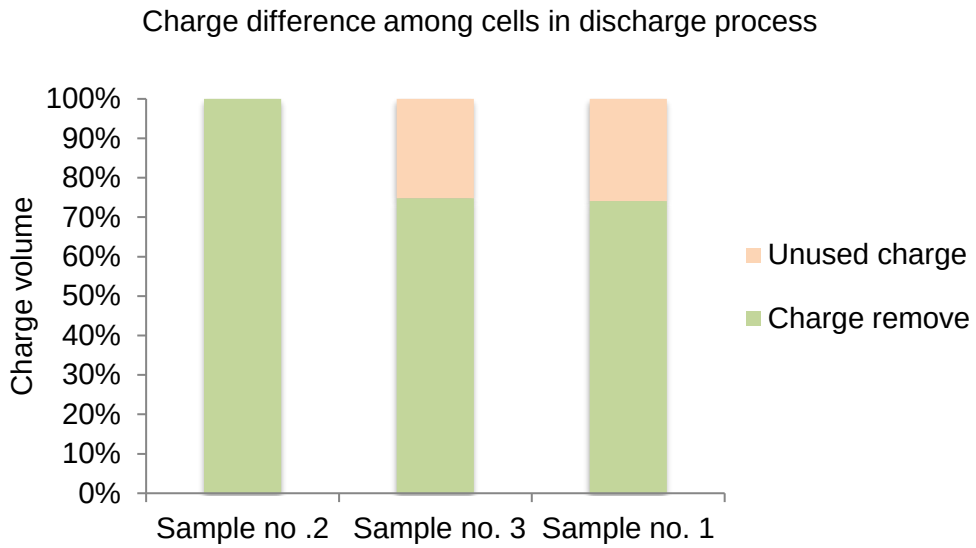

Figure 19: Charge difference in charging process among the three samples.

Figure 19 illustrates the remaining volume from the samples no. 1 and no. 3 when the sample no. 2 has reached its minimum voltage level.

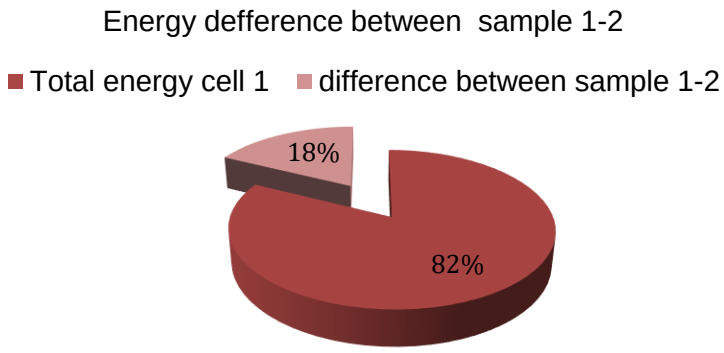

Figure 20: Energy losses for sample 1.

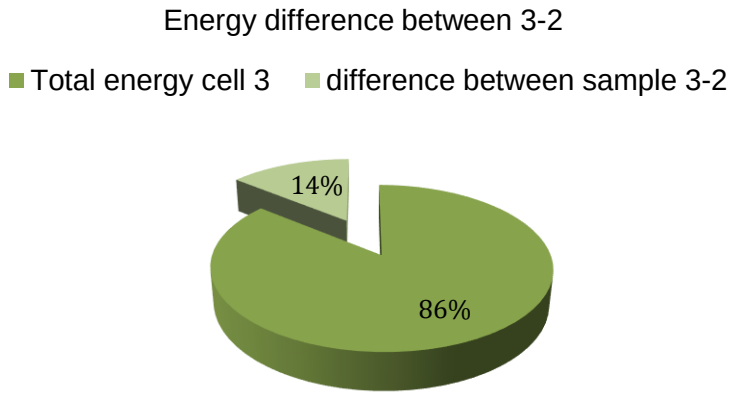

Figure 21: Energy losses for sample 3.

The Figure 20 and Figure 21 present the capacity, charge and energy wasted in the case of a passive balancing system used to equalize the cells. In other words, when the charge and discharge process is limited by the performance of the weakest cell within the system, the extra energy from the neighbouring cells is wasted as heat. In contrast, when an active balancing system is employed to balance the cells the extra energy removed from the higher cells is used to continue charging the weakest cell. This results in an increase of the charge and discharge time and energy efficiency.

For the case of sample no. 1, the energy losses within the passive system are up to 18% while for the sample no. 3 are about 14%. This means that sample no. 3 and no. 1 still have energy stored when the sample no. 2 is at the end of the discharge and the discharge process ends.

Finally, this energy discrepancy among cells results in an energy waste in case of a passive balancing system is placed for the whole system as Figure 22 shows. The total energy losses due to the imbalance between cells, reaches a value of 12% of the total energy stored in the whole system.

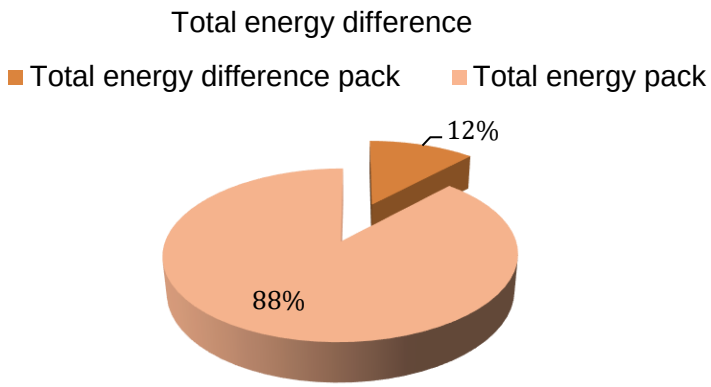

Figure 22: Total energy losses of the system.

We can define the energy efficiency of the two methods by studying the energy losses within the different systems as shown in Table 7.

Table 7: Summary of results from the passive and active BMS methods.

Methods	Passive	Active
Balancing current	0.000175	0.000175
Energy wasted (W)	9.5	-
Energy losses switches (W)	-	0.36
Cell degradation (A)	0.0003	-
Energy available (W)	60.5	70
Efficiency cell level	82%	99%
Efficiency system level	86%	99%

These results exemplify the energy losses within the BMS system and the total energy available while the balance among cells is in process.

5 Conclusions

It is evident that an electrical vehicle is built by several parts and devices. The replacement of some of these components with structural battery composites has the potential to reduce weight of about 20-30%. Since the structural battery composites can meet both the electrical and mechanical functions within the electric vehicle, substituting the traditional monofunctional materials results in a substantial increased drive range. As the comparative analysis of structural batteries shows, the more power supplied by structural batteries the more the drive range is increased. In fact, the drive range is increased by 23% if all the motor's propulsion supplied by the structural batteries compared to if it is supplied by traditional batteries. In this work the previous model has been improved to allow the analysis of the power supply, so that it meets the power needed by the motor. To accomplish this, the delivery of current is limited defining the available energy from the battery.

Looking at the demanded motor current, the peak current during the drive cycle never match the upper current limit value of the cell. This means that the battery pack can always deliver the instantaneous current required by the motor. Moreover, in case of a negative power demand, the current is cut off making the battery unavailable to deliver current. Furthermore, battery integrity and safety are maintained as the depth of discharge is not allowed to exceed 75% during the drive cycle.

The battery internal resistance limits the delivered current, and it was observed that this affects the gain in the drive range. The drive range is founded to decrease as the internal resistance increases. Consequently, any increase in the internal resistance of structural batteries compared with conventional batteries will impair drive performance.

The important of an active battery management system (BMS) implementation was demonstrated. The large variation in performance between cells requires the introduction of a BMS used to reduce the energy losses in structural batteries composite systems. Such BMS will reduce energy losses and cell degradation. The relevance of the BMS system has been validated with the energy efficiency analysis from the two different technologies. Here, the active balancing system presents an advantage from the passive system. According to the energy losses obtained, the active system is defined as an outstanding solution for the imbalance problems presented by the structural batteries technology.

6 Future work

While this current study has already demonstrated the potential of structural batteries covering the functions of conventional batteries and structural parts of the vehicle, some areas remain to be studied. Firstly, addressing the estimation of the battery power delivery we need a more accurate model for the electrical requirements prediction for structural batteries to improve their performance in the electric vehicle. In addition, an in-depth analysis of the overall stiffness of the structural battery composites is needed to allow their implementation in electric vehicle. Secondly, the internal effective resistance must be determined experimentally, to allow us to assess the structural battery characteristic even further. Lastly, the replacement of some vehicle parts with structural battery composites, needs an exhaustive analysis.

The BMS target design requires an in-depth study of the control system employed to predict and balance the cell differences. This will lead us to an optimization of the design, defining the suitable algorithms and communication system. Moreover, assessing the BMS by testing several structural batteries set in series and parallel will emphasise the relevance of the energy efficiency analysis performed in the current study. Furthermore, a thermal monitoring system is needed to prevent from thermal runaway during the structural batteries operation.

7 References

[1] International Energy Agency (IEA), "Global EV Outlook 2017: Two million and counting," *IEA Publications*, pp. 1–71, 2017.

[2] D. J. O'Brien, D. M. Baechle, and E. D. Wetzel, "Design and performance of multifunctional structural composite capacitors," *Journal of Composite Materials*, vol. 45, no. 26, pp. 2797–2809, 2011.

[3] AE Scholz. and E.S. Greenhalgh, "Feasibility Analysis and Comparative Assessment of Structural Power Technology in All-Electric Composite Aircraft, MSc Thesis," Imperial College London, 2017.

[4] G. Fredi *et al.*, "Graphitic microstructure and performance of carbon fibre Li-ion structural battery electrodes," *Multifunctional Materials*, no. 1, p. 015003, 2018.

[5] E. Jacques, M. H. Kjell, D. Zenkert, and G. Lindbergh, "Piezo-electrochemical effect in lithium-intercalated carbon fibres," *Electrochemistry Communications*, vol. 35, pp. 65–67, 2013.

[6] L. E. Asp and E. S. Greenhalgh, "Structural power composites," *Composites Science and Technology*, vol. 101, pp. 41–61, 2014.

[7] T. Carlson, "Multifunctional composite materials – design, manufacture and experimental characterisation," *Doctoral thesis*, Luleå University of Technology, Lulea, Sweden, 2013.

[8] S. Leijonmarck, T. Carlson, G. Lindbergh, L. E. Asp, H. Maples, and A. Bismarck, "Solid polymer electrolyte-coated carbon fibres for structural and novel micro batteries," *Composites Science and Technology*, vol. 89, pp. 149–157, 2013.

[9] E. L. Wong, D. M. Baechle, K. Xu, R. H. Carter, J. F. Snyder, and E. D. Wetzel, "Design and Processing of Structural Composite Batteries Engineering (SAMPE) 2007 Symposium and Exhibition," 2007, pp. 3–7.

[10] S. Ekstedt, M. Wysocki, and L. E. Asp, "Structural batteries made from fibre reinforced composites," *Plastics, Rubber and Composites*, vol. 39, pp. 148–150, 2010.

[11] D. Carlstedt, W. Johannisson, D. Zenkert, P. Linde, and L. E. Asp, "Conceptual Design Framework for Laminated Structural Battery Composites," 2018, European conference in composites materials, Athens Greece, pp. 24–28.

[12] J. Larminie and J. Lowry, *Electric Vehicle Technology Explained*. John Wiley & Sons, Ltd, 2003.

[13] R. Rangarajan, "Structural Battery Composites in Electric Vehicle Design, MSc Thesis," Chalmers University of Technology, 2018.

[14] A. F. Pacheco, M. E. S. Martins, and H. Zhao, "New European Drive Cycle (NEDC) simulation of a passenger car with a HCCI engine: Emissions and fuel consumption results," *Fuel*, vol. 111, no. 10, pp. 733–739, 2013.

[15] Y. Barsukov and Q. Jinrong, "Cell-balancing technics: Theory and implementation," in *Battery power management for portable deviices*, Boston: Artech house, 2013, pp. 111–138.

[16] M. Daowd, N. Omar, P. Van Den Bossche, and J. Van Mierlo, "A Review of Passive and Active Battery Balancing based on MATLAB/Simulink," *Interniona Review of electrical Egineering*, vol. 20, pp. 1–15, 2011.

[17] J. Gallardo-lozano, E. Romero-cadaval, M. I. Milanes-montero, and M. A. Guerrero-martinez, "Battery equalization active methods," *Journal of Power Sources*, vol. 246, pp. 934–949, 2014.

Appendix A BMS topologies

A. 1 Fixed resistor

Fixed resistor is the most straightforward equalization concept illustrated in **Error! Reference source not found.** A1. This method removes the excess energy from higher voltage cells by passing the current to the exposed to equalize them. It uses continued bypass of energy by adjusting the resistor to the cell voltage limit. This continued bypassing of energy results in a constant dissipation of heat, wasting energy [16].

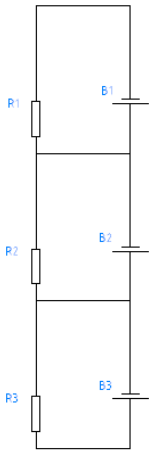

Figure A1: Architecture of fixed resistor.

A. 2 Shunt resistor

This method removes the energy using a resistor in series with a switcher set in parallel with each cell. This can be controlled using switches or relays in two modes [17]. One, where all relays are commanded by the same signal, in other words, they are switched on or off at the same time. While in the other, the voltage is monitored, and the switches are commanded individually. So when the imbalance is detected the correspondent switchers are selected bypassing the energy through the cell as it is illustrated in Figure A2. Like the previous one, this topology wastes the energy removed from the stronger cell as heat [16].

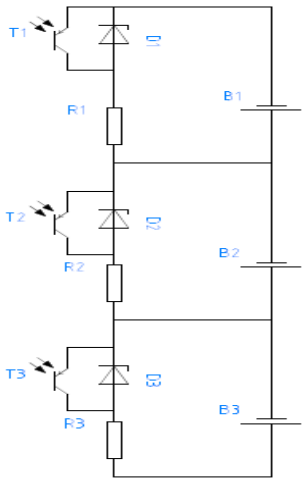

Figure A2: Shutting resistor.

A. 3 Cell to cell

This topology can be sub-divided in 5 main balancing methods using divergent technologies to make the balancing among cells.

First one is the switched capacitor illustrated in Figure A3 . The circuit required n-1 capacitors and 2n switches to make the balance between cells [16]. Within this method, two states are continually alternated. In the first state, the capacitor is switched with its corresponding upper cell, thus the capacitor is set to the voltage cell delivering or demanding from the mentioned cell. In the second state, the capacitors are set in parallel with the lower cell transporting or demanding energy from this one reaching its high voltage [17].

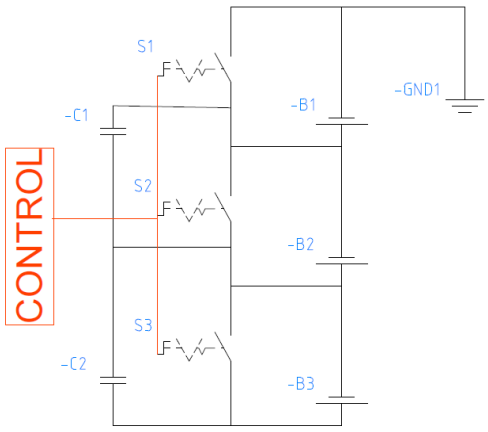

Figure A3: Switched capacitor architecture.

The second one is the double-tiered switched capacitor, this method uses two capacitors and 2n switches to balance n cells reducing the equalization time even to a quarter. This method also reduces the balancing time in comparison with other methods. The architecture used by this topology is illustrated in Figure A4.

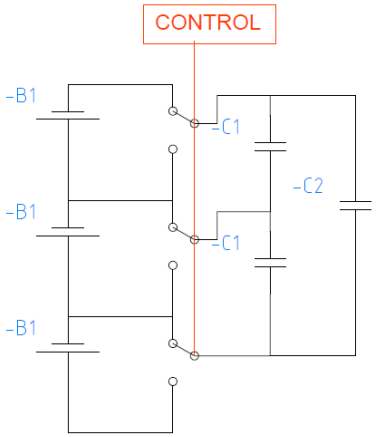

Figure A4: Double-tired capacitor architecture.

The third one is the cûk converter. In this topology, the two near cells are connected to an equalization module allowing the energy transfer from the cell with the highest voltage to the lowest through the transferring capacitor [17]. The topology of this method is shown in Figure A5.

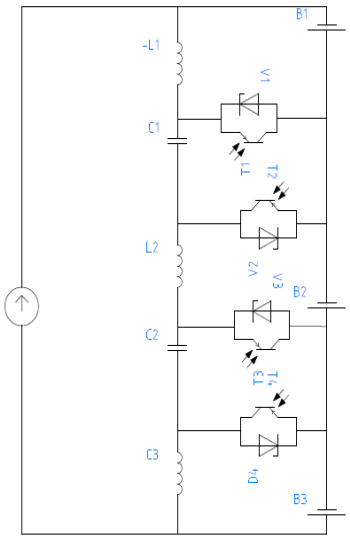

Figure A5: Cûk converter architecture.

Focusing on cells 1 and 2 and considering that the cell B1 is higher than the cell B2 as shows in **Error! Reference source not found.**. The following steps need to be executed to bypass the energy among cells. In the first period, the switcher T1 is switched off while the T2 is activated and the C1 capacitor is charged. In the second period, the switches T1 and T2 are turned on and off respectively and the energy stored in the capacitor is transferred to cell 2.

The fourth balancing method is the PWM controller converter. For this technology 3 topologies can be implemented, the basic one is shown Figure A6. In which, every module for equalization is connected across to each adjacent cell allowing next-to next energy transfer from the cell with the highest voltage to the cell with the lowest voltage. The energy is transfer first to the inductor where is storage and afterwards the inductance discharges the energy to the lowest voltage cell. The energy transfer and the current flow direction are effectuated by the corresponding transistors [17].

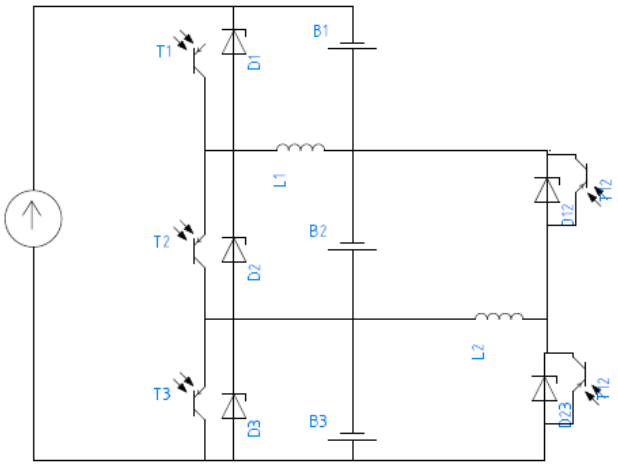

Figure A6: PWM controlled converter architecture.

The fifth method is the quasi-resonant and resonant converter. This both systems own similar architecture as the PWM controller shunting method. Each pair of balancing modules per cell is commanded by a PWM signal. The main difference is that this circuit employs a resonant circuit to move the energy to the neighboured cells formed by an inductor and a capacitor rather than an inductor as is illustrated in Figure A7. Indeed, the zero current switched function is achieved, using the symmetrical and bi-directional battery equalizers. As it can be appreciated, this method introduces a reduction of the switching losses. In the resonant hardware, a resistance circuit is employed instead of using intelligent control to monitor and generate the switchers PWM signals. This resonance circuit is employed to meet both functions, energy transfer and command the switchers at zero voltage.

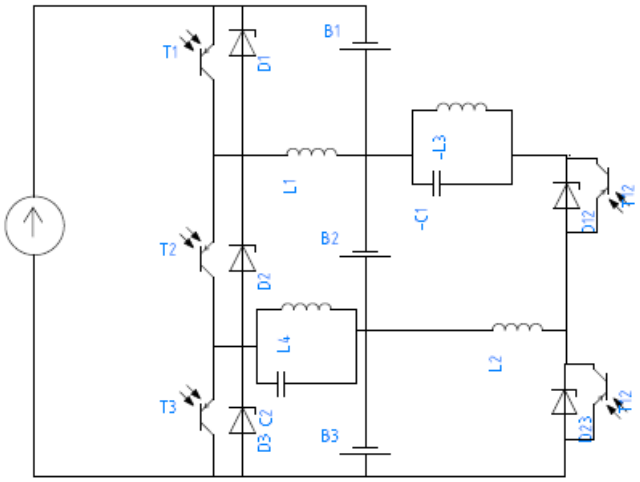

Figure A7: Quasiresonant converter architecture.

A. 4 Cell to pack

This method can be grouped in 5 different topologies shunt inductor, boost shunting, multiple transformers, multi-secondary winding transformer and switched transformer.

Shunt inductor

This configuration is illustrated in Figure A8. In case of a voltage difference between cells occurs, the inductor is alternately set in parallel activating the corresponding adjacent switchers of the cell with the whole pack.

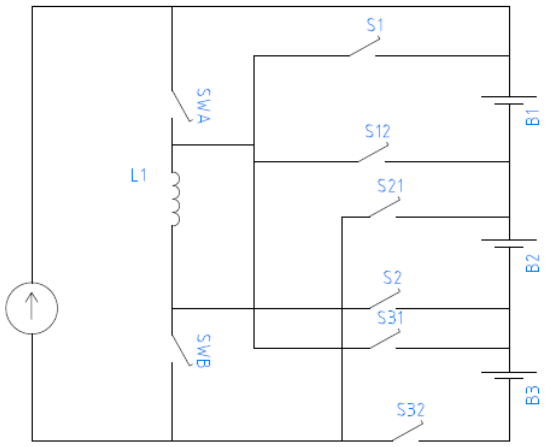

Figure A8: Shunt inductor architecture.

Boost shunting

Since the imbalance is detected, the corresponding switch together with the SWr switch commanded by the PWM signal, moving the energy to the nearby cells in the string. The architecture of this method is shown in Figure A9. Where the balancing module works as boost converter, increasing the voltage out-putt from the voltage input by using one transistor and a diode to save the energy remove from the strongest cell [17].

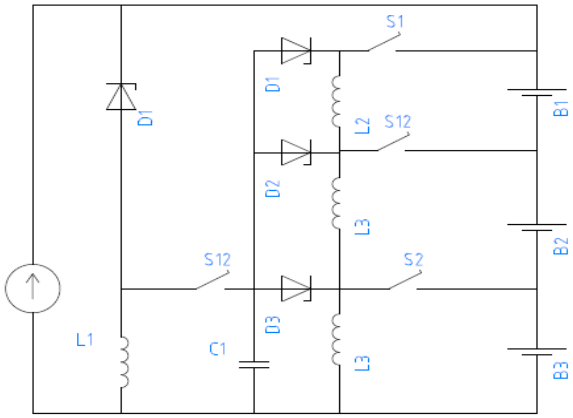

Figure A9: Boost shunting architecture.

Multiple transformers

A switch in series with the secondary side of the transformer is placed in parallel with each individual cell as Figure A10 shows. While the secondary sides of the transformers are set in parallel as well, resulting in a voltage converter insulated. Once one cell exceeds the voltage threshold, the energy is transferring to the pack by commanding the corresponding switch and therefore the corresponding DC/DC converter. There are two steps to carry out this process. First, the corresponding switch is turned on and the energy is saved into the inductor as a magnetic field. Afterwards, the corresponding switch is turned at the same time as the main switch as Figure A13 is turned on, allowing the energy flow through the primary side of the transformer and finally recovered to the whole battery pack [17].

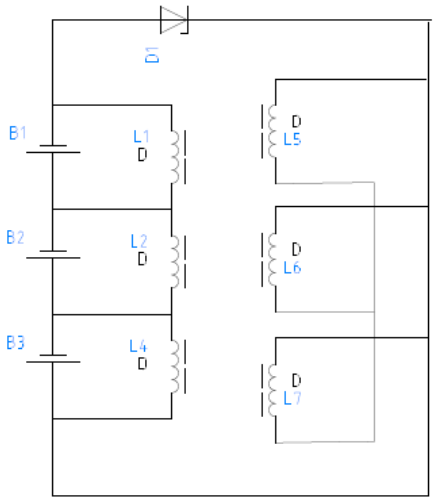

Figure A10: Multi-transformers architecture.

Multisecondary winding transformer

In case of the imbalance is detected, the switch associated with the highest voltage cell is switched and the current out to the cell starts to flow into the transformer [17]. Therefore, the extra energy is stored in the magnetic field. Once the process of energy stored is complete the corresponding switch is turned off and then the main switch is turned on, the energy is fed into the whole battery pack via the primary winding of the transformer as the Figure A11 shows.

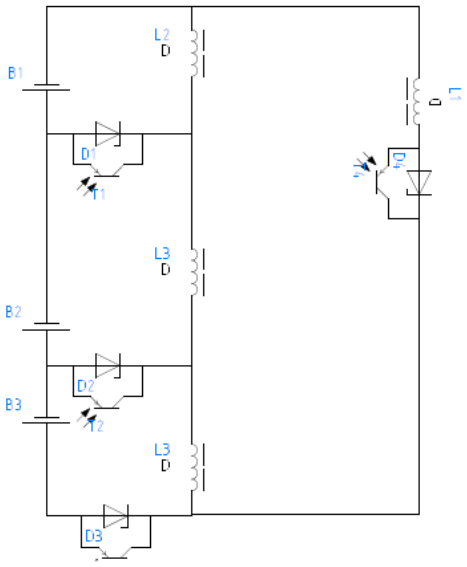

Figure A11: Multisecondary-winding transformer architecture.

Switched transformer

This method is very similar to the multisecondary winding transformer [17]. But in this case, the method employs only one switched transformer to transfer the energy from the whole battery pack to the lowest voltage cell through an array of switches, which selects the target cell that has to be equalized as illustrates Figure A12.

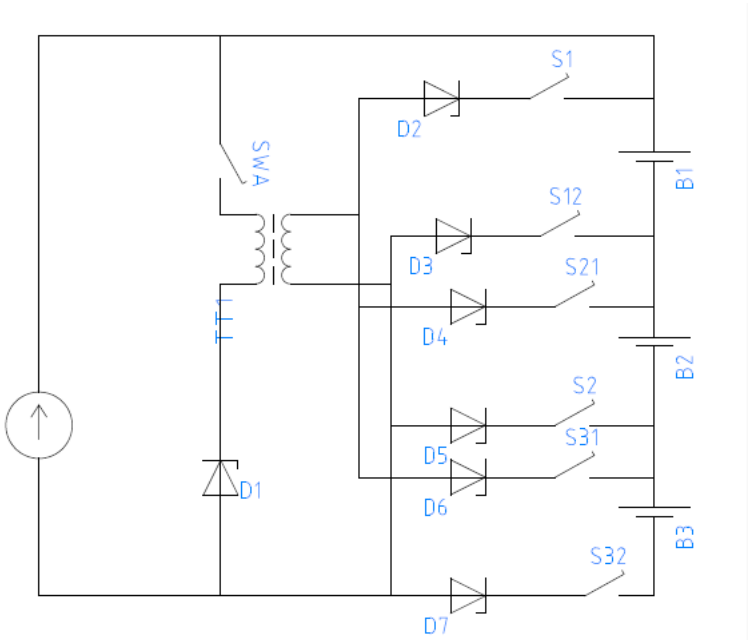

Figure A12: Switched transformer architecture.

A.5 Pack to cell

Voltage multiplier

In this method, two states are alternated continuously since the switch is controlled by squared signal. In the first stage, each cell is discharged through the even-numbered diodes, thus capacitors are charged. During the off period, the charge current is distributed among all the capacitors and through the diodes to the cells. These cells are charged less or more with respect to the voltage difference between cells [17]. This DC circuit is built with a current source, whose current is duty controllable and each cell is connected to the current source via two diodes an equivalent resistor as is illustrated in Figure A13.

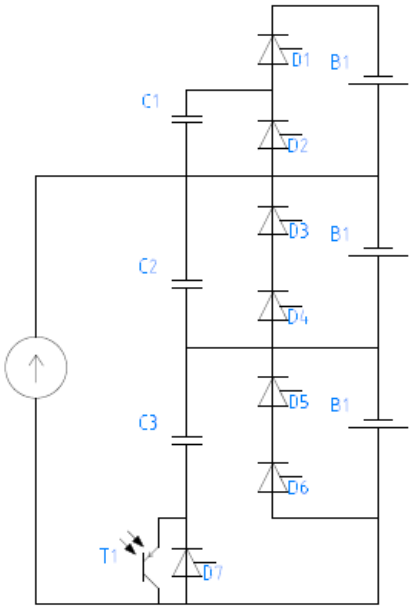

Figure A13: Voltage multiplier architecture.

Full-bridge converter

This method is based on the full-bridge PWM converters shown in Figure A14. According to the energy flow, the energy is transferred from the whole battery pack to the individual cells.

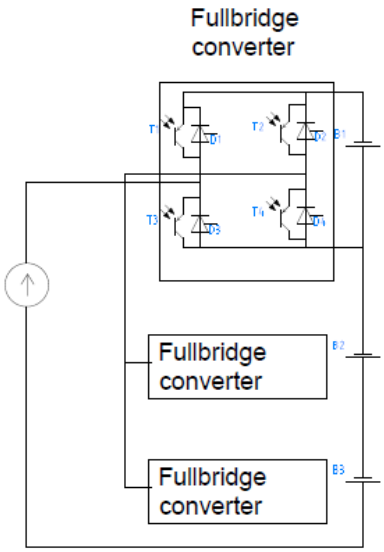

Figure A14: Full-bridge converter architecture.

Multi transformer

The charger is switched to the cells by the primary side of the transformer so that, the currents are induced to each secondary side. Leading to this, each cell will receive a current flow inversely proportional to its relative SOC. The balancing process is performed exemplified by Figure A15 in two steps. In the first step, the T1 switch is turned on and the primary winding reaches up to the current of the corresponding cell. Afterwards, the switch is turned off and the corresponding diode is turned on, thus the current flows into the target cell [17].

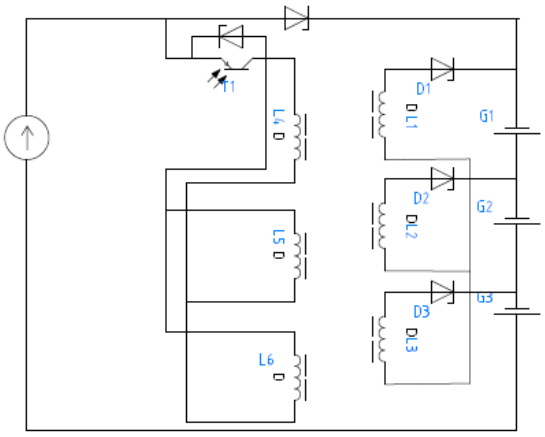

Figure A15. Multiple transformer pack to cell architecture.

Multisecondary winding transformer

Once the imbalance is detected the switch connected to the transformer primary winding is switched on, and hence the energy stored in the transformer. Afterwards, the switch is turned off and the energy is transfer to the secondary of the transformers. Most of this energy will be provided to the cell with the lowest voltage as Figure A16 shows.

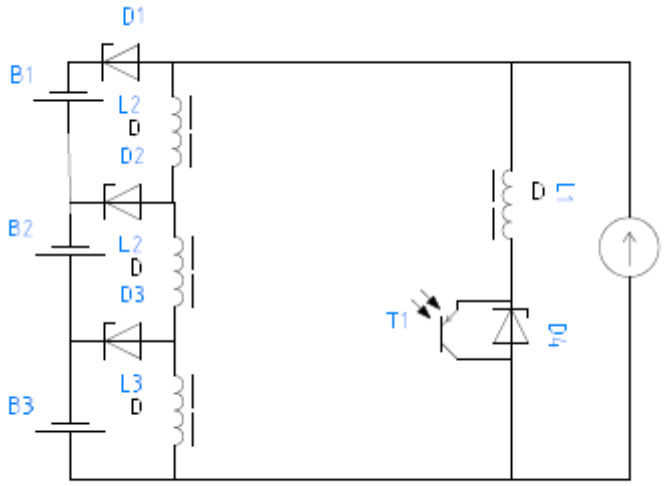

Figure A16: Multisecondary winding transformer pack to cell architecture.

Switched transformer

There are some similarities between this method and the multi-secondary winding transformer. In contrast, this method employs only one switched transformer to remove the energy from the whole battery pack to the lowest cell by several switches [17].

A. 6 Cell to pack to cell

This topology can be grouped into two different methods. First, the shared methods which transfer the energy from the most charged cells to a tank and returned the energy from the tank to the least charged cell within the battery pack, regardless of these cells are neighbours cells or not. The second group is formed by distributed methods. These methods make the equalization process in the two allowed direction, to equalize a cell from the energy pack and to equalize the pack from energy cell.

PWM controller converter

The cell balancing circuit composed by buck-boost converters which connect the stack cells with the capacitor tank. The buck-boost converter is formed by an inductor shared by the two converters mode, a capacitor, a diode, and a resistor as the Figure A17 illustrates. This circuit provides higher or lower voltage than the input depending on which mode is set by the transistor.

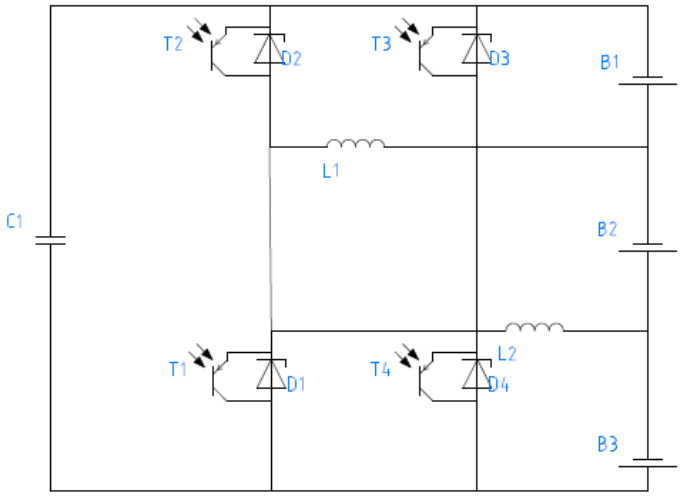

Figure A17: PWM controller converter cell to pack architecture.

Single switched capacitor

This method relays on the switched capacitor method shown in Figure A18. Firstly, the controller selects the corresponding pair of switches in parallel with the overcharged cell connecting it with the capacitor. Once the capacitor reaches the cell voltage, the controller selects the pair of switches in parallel with the target cell making the bridge between them with the capacitor and transferring the excess energy to the cell [17].

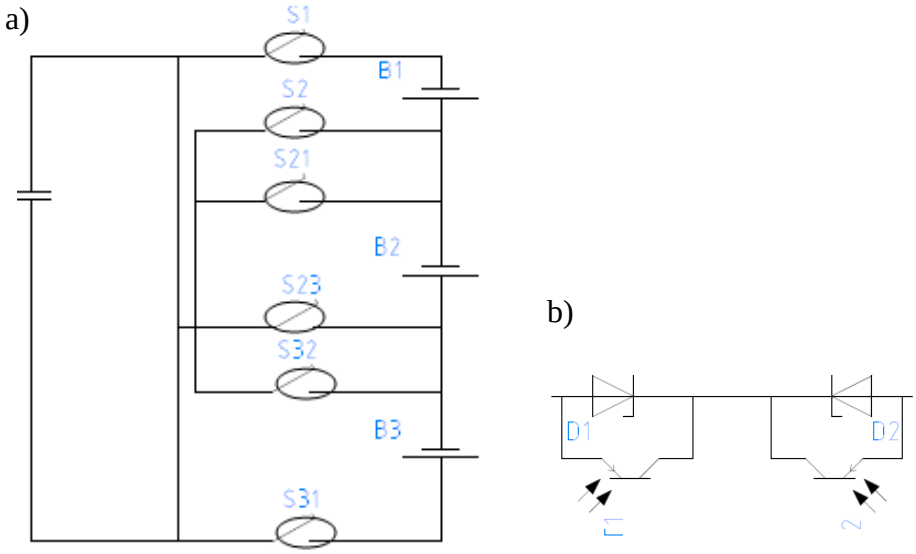

Figure A18: a) Single switched capacitor architecture b) Switch type.

Single switched inductor

As the single switched capacitor method, in this case, the controller selects first the pair of switchers delivering the energy to the inductor from the highest cell. Afterwards, the energy is

moved to the lowest cell by switching again the corresponding switchers as Figure A19 shows. [17].

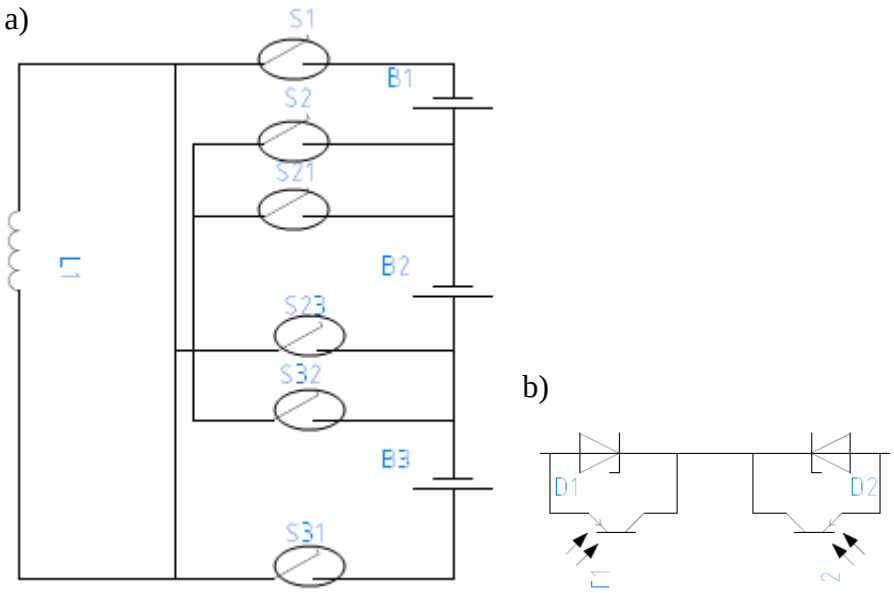

Figure A19: a) Single switched inductor architecture. b) Switch type.

Bidirectional multiple transformers

This method allows the transfer of energy in both directions, cell to pack and pack to cell. During the cell charging process, the energy is transferred from the pack to the cell, while the discharging the energy can be transferred from the pack to the weakest cell. This method combines the different advantages of the multiple transformers method as it is shown in Figure A20.

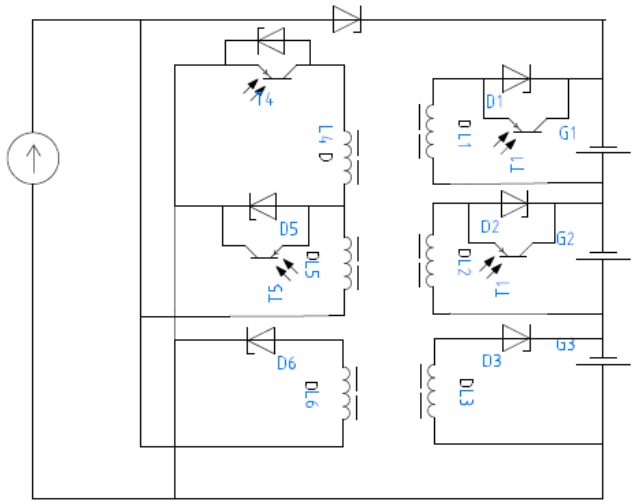

Figure A20: Bidirectional multi-transformer architecture.

Bidirectional multi-secondary winding transformer.

In this method, each cell is in parallel with a switch and an inductor as shows Figure A21. This method allows to use different control types. The first control transfers the energy from the pack to the weakest cell by activating the switch linked to the primary winding. Then the switchers from this site are set off and the corresponding switches to the cells are activated. The other control mode allows the energy transfer from the most charged cell to the rest of the stack cells, by switching the corresponding switch of the target cell allowing the transfer of energy to the primary side of the transformer. Resulting in a directly migration of energy most of it to the weakest cell.

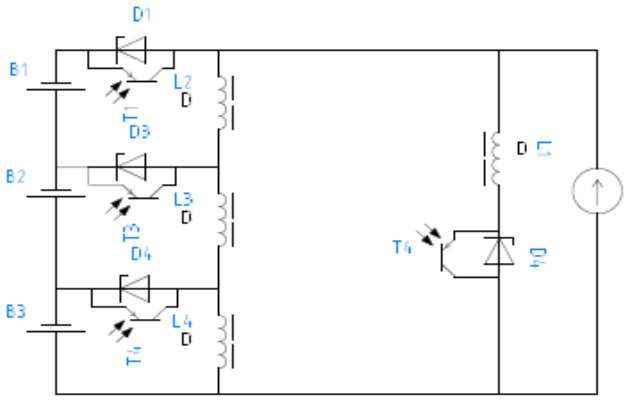

Figure A21: Bidirectional multisencondary winding transformer architecture.

Bidirectional switched transformer

A single transformer is used to allow the energy transfer from the most charged cell to the pack or from the pack to the weakest cell by selecting the corresponding switches. The diagram of the topology is shown in Figure A22.

a)

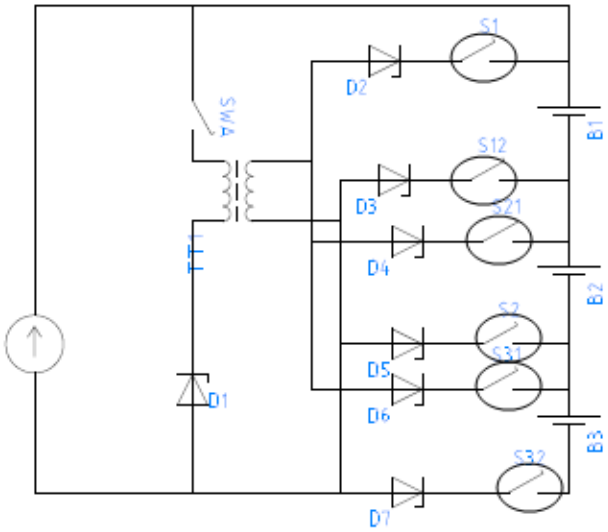

b)

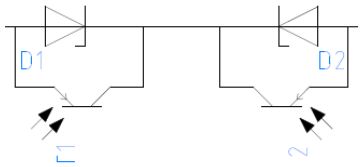

Figure A22: a) Bidirectional switched transformer. b) Switch type.

Table A1: Strategies for the BMS (1).

Topology	Fixed resistor	Shunt resistor	Switched capacitor	Double tired switcher capacitor	Cûk converter
Kind	Passive	Passive	Active	Active	Active
Circuit elements used	Fixed resistor	Variable resistor	Capacitor	Capacitor	Capacitor
Charge-discharge technique	Unidirectional	Unidirectional	Bidirectional	Bidirectional	Bidirectional
Applications	Low power	Low power	High power	High power	High power
Efficiency	Low	Low	High	High	50% Best case
Best effective period	None	One mode	Both modes are effective	Both modes are effective	One mode
Speed	None	High	Low	Medium	Medium
Complexity	None	Low	Low	Low	High
Cost	Cheap	Cheap	Cheap	Medium	Medium

Table A2: Strategies for the BMS (2).

Topology	PWM controller converter	Quasiresonant and resonant converter	Shunt inductor	Boost shunting	Multiple transformers
Kind	Active	Active	Active	Active	Active
Circuit elements used	Inductor	Inductor	Inductor	Boost converter	Transformer
Charge and discharge technique	Bidirectional	Bidirectional	Bidirectional	Bidirectional	Bidirectional
Applications	High power	High power	High power	High power	High power
Efficiency	50 % Best case	50 % Best case	50 % Best case	50 % Best case	Low
Best effective period	One mode	One mode	One mode	One mode	One mode
Speed	Medium	Medium	Low	Medium	Medium
Complexity	High	High	High	High	High
Cost	Medium	Expensive	Medium	Medium	Expensive

Table A3: BMS topologies (3).

Topology	Multisecondary winding transformer	Switched transformer	Voltage multiplier	Full-bridge converter	Multiple transformers
Kind	Active	Active	Active	Active	Active
Circuit elements used	Transformer	Transformer	Diodes and capacitors	Converter	Transformer
Charge and discharge technique	Bidirectional	Bidirectional	Bidirectional	Bidirectional	Bidirectional
Applications	High power	High power	High power	High power	High power
Efficiency	Low	Low	High	High	Low
Best effective period	One mode	One mode	One mode	One mode	One mode
Speed	Low	Low	Medium	High	Medium
Complexity	High	High	Low	Medium	Low
Cost	Expensive	Expensive	Cheap	Expensive	Expensive

Table A4: BMS topologies (4).

Topology	Multisecondary winding transformer	Switched transformed	PWM controller	Single switched capacitor	Single switched inductor
Kind	Active	Active	Active	Active	Active
Circuit elements used	Transformer	Transformer	Buck-boost converter	Capacitor	capacitor
Charge and discharge technique	Bidirectional	Bidirectional	Bidirectional	Bidirectional	Bidirectional
Applications	High power	High power	High power	High power	High power
Efficiency	Low	Low	50% Best case	High	50% Best case
Best effective period	One mode	One mode	One mode	Both modes are effective	Both modes are effective
Speed	Medium	Low	Medium	Low	Low
Complexity	Low	High	High	High	High
Cost	Expensive	Expensive	Expensive	Cheap	Medium

Table A5: BMS topologies (5).

Topology	Bidirectional multiple transformers	Bidirectional multisecundary winding transformer	Bidirectional switched transformer
Kind	Active	Active	Active
Circuit elements used	Transformer	Transformer	Transformer
Charge and discharge technique	Bidirectional	Bidirectional	Bidirectional
Applications	High power	High power	High power
Efficiency	Low	Low	Low
Best effective period	One mode	One mode	One mode
Speed	Medium	Medium	Medium
Complexity	High	High	High
Cost	Expensive	Expensive	Expensive